Global Assessment of the Standardized Evapotranspiration Deficit Index (SEDI) for Drought Analysis and Monitoring

SERGIO M. VICENTE-SERRANO,[a] DIEGO G. MIRALLES,[b] FERNANDO DOMÍNGUEZ-CASTRO,[a] CESAR AZORIN-MOLINA,[c] AHMED EL KENAWY,[a,d] TIM R. MCVICAR,[e,f] MIQUEL TOMÁS-BURGUERA,[g] SANTIAGO BEGUERÍA,[g] MARCO MANETA,[h] AND MARINA PEÑA-GALLARDO[a]

[a] *Instituto Pirenaico de Ecología, Spanish National Research Council, Zaragoza, Spain*
[b] *Ghent University, Ghent, Belgium*
[c] *Regional Climate Group, Department of Earth Sciences, University of Gothenburg, Gothenburg, Sweden*
[d] *Department of Geography, Mansoura University, Mansoura, Egypt*
[e] *CSIRO Land and Water, Canberra, Australian Capital Territory, Australia*
[f] *Australian Research Council Centre of Excellence for Climate System Science, University of New South Wales, Sydney, New South Wales, Australia*
[g] *Estación Experimental de Aula Dei, Spanish National Research Council, Zaragoza, Spain*
[h] *Department of Geosciences, University of Montana, Missoula, Montana*

(Manuscript received 15 November 2017, in final form 28 March 2018)

ABSTRACT

This article developed and implemented a new methodology for calculating the standardized evapotranspiration deficit index (SEDI) globally based on the log-logistic distribution to fit the evaporation deficit (ED), the difference between actual evapotranspiration (ETa) and atmospheric evaporative demand (AED). Our findings demonstrate that, regardless of the AED dataset used, a log-logistic distribution most optimally fitted the ED time series. As such, in many regions across the terrestrial globe, the SEDI is insensitive to the AED method used for calculation, with the exception of winter months and boreal regions. The SEDI showed significant correlations ($p < 0.05$) with the standardized precipitation evapotranspiration index (SPEI) across a wide range of regions, particularly for short (<3 month) SPEI time scales. This work provides a robust approach for calculating spatially and temporally comparable SEDI estimates, regardless of the climate region and land surface conditions, and it assesses the performance and the applicability of the SEDI to quantify drought severity across varying crop and natural vegetation areas.

1. Introduction

Drought is usually considered as a period of abnormally low water supply that fails to satisfy the existing demands of different natural systems and socioeconomic sectors. This situation is usually caused by a prolonged period of below-average precipitation. It is well known that drought is difficult to identify and quantify over space and time, which makes it one of the most complex natural hazards (Wilhite 1993, 2000; Vicente-Serrano 2016). This is particularly so because according to most definitions of drought, with the exception of those that focus exclusively on meteorological aspects, droughts are impact-dependent phenomena that affect a diverse range of natural and socioeconomic variables (Lloyd-Hughes 2014; Van Loon 2015). Moreover, the degree of vulnerability and the capacity of recovery to drought occurrence strongly differ among regions as a function of their background socioeconomic and environmental characteristics (Simelton et al. 2009; Choat et al. 2012; Antwi-Agyei et al. 2012; Yang et al. 2017). Therefore, drought severity depends on meteorological conditions (e.g., magnitude and duration of precipitation shortage) and is also impacted by several human and environmental factors, such as land use or risk management (Van Loon et al. 2016).

However, the quantification of drought severity based on its impacts is a challenge, given the spatial differences, the sector of interest, and the availability of

Supplemental information related to this paper is available at the Journals Online website: https://doi.org/10.1175/JCLI-D-17-0775.s1.

Corresponding author: Sergio M. Vicente-Serrano, svicen@ipe.csic.es

DOI: 10.1175/JCLI-D-17-0775.1

impact data (Stahl et al. 2015, 2016). For these reasons, scientists, managers, and policy-makers usually quantify drought based on climate information only (McKee et al. 1993; Vicente-Serrano et al. 2010a): the most widely used drought metrics are generally based on climate information available across the globe. Overall, the potential of drought indices is particularly related to the possibility of quantifying drought severity and comparing their climate component both spatially and temporally. A detailed review of current climate drought indices can be found in Heim (2002), Keyantash and Dracup (2002), and Mishra and Singh (2010).

Being inexpensively and widely observed, precipitation is usually employed as the key input variable in traditional drought indices (e.g., Palmer 1965; McKee et al. 1993). However, precipitation is only one of the multiple variables that control water stress conditions in natural ecosystems and affect water availability in usable water stores (e.g., soil moisture, streamflow, reservoir storage, and lake water). Water shortage is ultimately dependent on the input of water through precipitation, lateral inflows, melting, or irrigation and is also crucially regulated by the atmospheric evaporative demand (AED), that is, the potential of the lower atmosphere to receive water via evapotranspiration from the abovementioned terrestrial water stores. Under low soil moisture, rising AED rates further increases vegetation water stress (e.g., Ciais et al. 2005; McDowell et al. 2008; Zampieri et al. 2009), causing stomata closure and the collapse of the photosynthetic machinery potentially resulting in crop failure (Lobell et al. 2011; Asseng et al. 2015) and forest decay and mortality (Allen et al. 2015; Anderegg et al. 2013; Breshears et al. 2013).

Numerous studies have demonstrated the importance of AED in triggering drought or intensifying drought severity (e.g., Ciais et al. 2005; Otkin et al. 2016). For these reasons, several drought indices use AED in their formulations. For example, compared to precipitation-based drought indices such as the standardized precipitation index (SPI) (McKee et al. 1993), the standardized precipitation evapotranspiration index (SPEI) (Vicente-Serrano et al. 2010a), which is obtained by means of the standardization of the difference between precipitation and AED at different time scales, has shown better performance in terms of identifying drought impacts in a variety of drought-prone systems and regions across the globe (Vicente-Serrano et al. 2012a; McEvoy et al. 2012; Wang et al. 2006; Chen et al. 2016; Labudova et al. 2017). In fact, it has been suggested that the AED may be the single most useful variable to quantify drought severity (McEvoy et al. 2016a). Accordingly, drought indices based only on AED have been recently formulated under the premise that AED anomalies are strongly connected, via a complementary relationship, with precipitation, soil moisture, and actual evapotranspiration (ETa) anomalies (Hobbins et al. 2016; McEvoy et al. 2016b).

Here, a conceptual distinction between AED and ETa must be established. There are different forms to determine AED, among them pan evaporation (the evaporation from a pan full of water) or crop reference evapotranspiration (ETo; the ETa of a hypothetical unstressed alfalfa grassland of uniform height with a closed canopy so the soil is shaded), which can be compared spatially since its calculation only depends on meteorological inputs (Katerji and Rana 2011). Independent of the choice of these definitions, AED does not directly depend on the actual water storage in land, and it is thus different from the ETa, which is the volume of water that is actually evaporated directly from soil, water and vegetation surfaces and/or transpired from vegetation into the atmosphere. While there are no water constraints for evaporation under humid conditions, ETa is constrained mainly by soil water availability (and ultimately by precipitation) in dry environments (Budyko 1948). As such, the use of drought indices that account only for AED is inappropriate in regions with nonconstraining soil moisture conditions, given that a positive AED anomaly cannot be representative of drought severity. In such regions, water stress conditions are likely better quantified considering both AED and ETa.

From agronomic and ecophysiological perspectives, the evaporation deficit (ED), defined as the difference between ETa and AED, is more relevant than considering ETa or AED separately. Regardless of the climate regime, high ED causes stomatal closure, thus a decrease in the photosynthetic activity, carbohydrate accumulation, and net primary production (Leuning 1995; Brümmer et al. 2012; Vicente-Serrano et al. 2015). If the ED is very high and wilting point is reached, plants may die as a result of vascular damage (Will et al. 2013; Anderegg et al. 2015). Under the aforementioned assumptions, the ED has been proposed for quantifying drought severity (Narasimhan and Srinivasan 2005; Yao et al. 2010; Anderson et al. 2011; Kim and Rhee 2016). Unlike AED, which can be calculated by means of relatively simple physically based models (e.g., Penman 1948; Allen et al. 1998; Rotstayn et al. 2006), the calculation of ETa is subject to many sources of uncertainty. ETa depends on a wide range of factors, including, but not limited to, AED, soil water availability, soil characteristics, vegetation morphology, physiology and phenology, and the complex relationships existing between these factors (Morton 1983).

Recently, the availability of remote sensing data and surface–atmosphere models has allowed for the development of global ETa products (Allen et al. 2007; Fisher

et al. 2008; Mu et al. 2011; Miralles et al. 2011; Zhang et al. 2016). Similarly, drought indices have been developed based on the ED, mainly to analyze natural vegetation and crop stress; for instance, Anderson et al. (2011), Yao et al. (2010), and Mu et al. (2011) developed different normalized drought indices [e.g., the evapotranspiration deficit index (EDI) and the evaporative stress index (ESI)] by means of observational meteorological data and space-based products to estimate ED. Following the same rationale, Kim and Rhee (2016) proposed the standardized evapotranspiration deficit index (SEDI) using ETa data estimated based on Bouchet's (1963) complementary hypothesis and used an approach widely used to calculate a drought index comparable spatially and temporally (e.g., the SPI and the SPEI). Here, we follow the same nomenclature proposed by Kim and Rhee (2016) to refer to a standardized drought index based on the ED.

It is expected that future improvements on ETa estimates based on remote sensing data and model output will increase the use of ETa for analyzing and monitoring drought at large scales (Fisher et al. 2017). Our definition of SEDI allows for a straightforward utilization of these estimates. Yet, it is necessary to develop robust statistical calculation procedures and to comprehensively evaluate the usefulness of this indicator in comparison to other available drought indices.

Our overarching goal is to provide a metric using ED to quantify drought severity and make robust spatial and seasonal comparisons. Our specific objectives are to (i) find a robust probability distribution to fit the ED series worldwide to calculate the SEDI; (ii) compare the impact of different AED estimations on the SEDI; (iii) compare the SEDI time series at the global scale with another widely used drought index that accounts for precipitation and AED, namely, the SPEI; and (iv) assess the skill of the SEDI in terms of determining vegetation activity anomalies globally.

2. Data

a. Actual evapotranspiration

We used ETa estimates from the Global Land Evaporation Amsterdam Model (GLEAM) version 3a (v3a). Full details about the development and characteristics of this dataset are found in Miralles et al. (2011) and Martens et al. (2017). GLEAM is a methodology dedicated to deriving evaporation from satellite observations of its main drivers. Interception loss is independently calculated using Gash's (1979) analytical model forced by observations of precipitation and vegetation cover while the remaining evaporation components use Priestley and Taylor's (1972) potential evaporation formulation constrained by a multiplicative stress factor. For transpiration and soil evaporation, this stress factor is calculated based on the content of water in vegetation (microwave vegetation optical depth) and root zone (multilayer soil model driven by observations of precipitation and updated through assimilation of microwave surface soil moisture).

Actual evaporation estimates from GLEAM have been validated against eddy covariance towers worldwide, and errors have been estimated base on triple collocation analysis. Miralles et al. (2011) reported average correlations of 0.83 and 0.90 for daily and monthly estimates, respectively, and an average root-mean-square difference (RMSD) of approximately 0.3 mm day^{-1} for in situ validations against 43 eddy covariance towers. More recently, Martens et al. (2017) reported a mean correlation of 0.81–0.86 based on 91 eddy covariance towers. In addition, GLEAM output has shown a better performance than other available evaporation datasets to close the water balance over a wide range of hydrological catchments, a better agreement with the expectations from the Budyko framework, and a good skill to partition evaporation fluxes into transpiration, interception, and bare soil evaporation (Michel et al. 2016; Miralles et al. 2016). GLEAM datasets are openly available globally at daily temporal resolution and 0.25° spatial resolution for 1980–2016 (https://www.gleam.eu/#downloads). Here, we aggregated the data to monthly 0.5° resolution.

b. Atmospheric evaporative demand and precipitation

To assess the sensitivity of SEDI to different AED inputs, two AED datasets were used: 1) GLEAM v3a (Miralles et al. 2011; Martens et al. 2017) and 2) Climatic Research Unit (CRU) time series (TS), version 3.24.01 (Harris et al. 2014). GLEAM calculates Priestley and Taylor's (1972) potential evapotranspiration (ETp), which is only forced by incoming radiation and air temperature, and here are used as a proxy of AED. The CRU TS AED is estimated by Allen's et al. (1998) FAO-56 ETo Penman–Monteith equation, which is simplified by assuming spatiotemporally constant wind speed (Harris et al. 2014). For the calculation of SPEI we used the analogous CRU TS precipitation dataset.

c. Global GIMMS NDVI

To compare the SEDI spatiotemporal variability with the anomalies of vegetation activity that could be related to drought severity conditions, a metric of vegetation activity based on satellite data was used. For this purpose, we used the normalized difference vegetation

index (NDVI) dataset (3g.v1) developed by the Global Inventory Monitoring and Modeling System (GIMMS) observed by AVHRR sensors on board NOAA satellites (Pinzon and Tucker 2014), which Beck et al. (2011) demonstrated was the optimal AVHRR-NDVI dataset for time series analysis. The NDVI exhibits a strong relationship with vegetation parameters such as green biomass (Tucker et al. 1983; Gutman 1991) and fractional vegetation cover (Gillies et al. 1997; Duncan et al. 1993). NDVI has long been used to analyze drought impacts on vegetation (Liu and Kogan 1996; Kogan 1997; McVicar and Jupp 1998; Ji and Peters 2003; Vicente-Serrano et al. 2013; Papagiannopoulou et al. 2017). The NDVI dataset is monthly at 0.5° resolution over 1981–2014. To facilitate a direct comparison between the NDVI and SEDI in both space and time, the NDVI series were standardized by fitting the monthly NDVI series to a log-logistic distribution and the cumulative probabilities were transformed to standardized units following the same approach used for the SPI and the SPEI (Vicente-Serrano 2006; Vicente-Serrano et al. 2010a).

3. Methods

a. *Calculation of the evapotranspiration deficit from the gridded global data*

Recall that we define the ED as ETa minus AED. Two versions of monthly ED were calculated; both used monthly GLEAM ETa estimates with AED formulations from 1) CRU TS version 3.24.01 ETo and 2) GLEAM ETp. These calculations were performed for the terrestrial globe excluding the warm desert areas and Antarctica and Greenland, where several methodological limitations exist (Fisher et al. 2011; Beguería et al. 2014). Figure S1 in the supplemental material illustrates the spatial averages and standard deviations of the ED in representative months of the four seasons of the year, and Fig. S2 shows the temporal evolution of the ED in some world regions.

b. *Assessment of different probability distributions to calculate the SEDI*

Eight probability distributions were tested [general extreme value (GEV), log-logistic, lognormal, Pearson III, generalized Pareto, Weibull, normal, and exponential distributions] to transform ED values to a standardized normal variable (i.e., SEDI). These statistical distributions have been widely used to standardize numerous hydrological and meteorological variables (e.g., Vicente-Serrano et al. 2012b; Stagge et al. 2015), being a common tool to calculate spatially and temporally comparable drought indices using either precipitation, AED, or both (e.g., McKee et al. 1993; Vicente-Serrano et al. 2010a; Ma et al. 2014; Hobbins et al. 2016). Unfortunately, no previous studies have tested the goodness of these distributions to fit ED values. Since the use of different probability distributions may produce substantial differences in the resulting drought indices (e.g., Stagge et al. 2015; Vicente-Serrano and Beguería 2016), we calculated 16 different global SEDI datasets, each one using one of the aforementioned probability distributions and the two different AED datasets (CRU TS version 3.24.01 and GLEAM). Following Hosking (1990), the parameters of the distributions were calculated using unbiased probability weighted moments (UB-PWMs). Calculations were performed independently for each ED monthly series to account for the strong seasonality of ED in the majority of the world climates. Once the monthly ED series were fit to a probability distribution, cumulative probabilities of the ED values were obtained and transformed to standardized units (SEDI). For this purpose, the classical approach of Abramowitz and Stegun (1965) was used, which is also used for calculating other drought indices such as the SPI and the SPEI.

Similar to the SPI handling of months with no precipitation, the calculation of ED also considers the case of months with ED = 0.0 mm month^{-1}. This occurs when ETa equals AED. In humid and cold regions these conditions can occur frequently during winter months, even at monthly time scales, given that ETa tends to approach AED and there is adequate water availability to satisfy ETa (because of low AED) of these regions at these times. To cope with zero values, we implemented Stagge et al.'s (2015) approach to calculate the SPI, which is based on the ''center of mass'' of the zero distribution rather than the maximum probability.

The UB-PWMs calculation of each monthly ED series requires a minimum of three values larger than zero in the entire multiannual record. In large areas of the Northern Hemisphere, ED is likely to be zero during the winter months, which makes it impossible to define the SEDI in these months and regions. Additionally, an SEDI calculation based on some of the eight tested probability distributions is not possible in some cases because the parameters of that specific distribution cannot be fitted to the ED data. Moreover, in a few cases, the origin parameter of the distribution can be higher than the lowest observed ED values, indicating no solution for the SEDI in these cases.

To assess the performance and robustness of the eight probability distributions used for the calculation of the SEDI, we first calculated the percentage of monthly ED series that cannot be fitted by each of them, and

TABLE 1. Percentage of monthly time series of ED with no fitting solution tested with the eight probability distributions.

	Log-logistic		GEV		Lognormal		Pearson III		Weibull		Generalized Pareto		Normal		Exponential	
Month	GLEAM	CRU	GLEAM	CRU	GLEAM	CRU	GLEAM	CRU	GLEAM	CRU	GLEAM	CRU	GLEAM	CRU	GLEAM	CRU
Jan	34.6	15.4	34.6	15.4	77.9	68.8	34.6	15.4	62.4	38.3	34.6	15.4	31.6	12.9	31.6	12.9
Feb	13.9	2.9	13.9	2.9	74.5	67.9	13.9	2.9	49.4	30.5	13.9	2.9	12.1	1.8	12.1	1.8
Mar	5.2	1.9	5.2	1.9	63.9	66.7	5.2	1.9	34.2	22.9	5.2	1.9	4.8	1.6	4.8	1.6
Apr	2.5	0.4	2.5	0.4	58.0	63.7	2.5	0.4	29.5	17.7	2.5	0.4	2.2	0.3	2.2	0.3
May	0.4	0.3	0.4	0.3	59.9	57.3	0.4	0.3	27.8	11.7	0.4	0.3	0.4	0.2	0.4	0.2
Jun	0.7	0.9	0.7	0.9	66.6	58.1	0.7	0.9	35.0	12.6	0.7	0.9	0.7	0.7	0.7	0.7
Jul	0.6	0.8	0.6	0.8	69.6	60.6	0.6	0.8	40.6	15.6	0.6	0.8	0.5	0.6	0.5	0.6
Aug	1.6	0.3	1.6	0.3	69.7	61.0	1.6	0.3	46.7	15.9	1.6	0.3	1.4	0.2	1.4	0.2
Sep	4.4	0.3	4.4	0.3	68.9	56.9	4.4	0.3	46.9	10.6	4.4	0.3	4.2	0.2	4.2	0.2
Oct	19.2	0.8	19.2	0.8	72.1	57.0	19.2	0.8	49.9	17.7	19.2	0.8	18.4	0.4	18.4	0.4
Nov	37.6	5.8	37.6	5.8	77.7	66.3	37.6	5.8	61.0	30.8	37.6	5.8	36.2	4.4	36.2	4.4
Dec	43.3	13.7	43.3	13.7	81.3	68.0	43.3	13.7	67.2	38.9	43.3	13.7	41.6	10.1	41.6	10.1

distributions with high percentages were discarded (usually >50%; see Table 1). With the remaining distributions, the normality of the resulting SEDI series across the terrestrial globe at each 0.5° resolution pixel was tested. Stagge et al. (2015) applied the Shapiro–Wilks (SW) test to determine whether the standardized variable (i.e., the SEDI) follows a standard normal distribution. The advantage of this test is that the parameter values are known beforehand and not computed from the input data. The p values of the SW test for each of the monthly global SEDI series obtained with the eight probability distributions were calculated. A rejection rate of $p < 0.05$ (corresponding to 95% confidence level) was used to discriminate the SEDI series that follow a normal standard variable.

Nevertheless, as shown by Vicente-Serrano and Beguería (2016), it is difficult to define the "best" candidate distribution to calculate a standardized drought index, as the application of the SW goodness-of-fit test to evaluate the goodness of a distribution is limited at the tails of the distribution that are the most relevant values for a drought index. For this reason, we also analyzed the frequencies of high and low SEDI values obtained by the eight probability distributions and compared the associated return periods.

c. *Comparison between SEDI obtained from two different AED datasets and between SEDI and SPEI*

SEDI calculated using the CRU TS and GLEAM AED datasets were compared by means of the per-pixel Pearson's correlation coefficient considering the different monthly series.

d. *Comparison between SEDI and SPEI*

The SPEI at time scales ranging between 1 and 24 months was calculated using CRU TS monthly precipitation and GLEAM AED data for 1981–2014. For this purpose, a log-logistic distribution and UB-PWMs were used [see details in Vicente-Serrano et al. (2010a), Beguería et al. (2014), and Vicente-Serrano and Beguería (2016)]. For each pixel, we calculated the SPEI time scale that had the highest correlation with the SEDI for the different monthly series. Regardless of the SPEI time scale, we also calculated the spatial distribution of the maximum correlation between SPEI and SEDI.

e. *Assessing the skill of the SEDI and SPEI in identifying spatiotemporal anomalies of vegetation state*

Finally, the relationship between the standardized NDVI (sNDVI) and the SEDI and SPEI using Pearson's correlation coefficients was calculated. As the global

TABLE 2. Percentage of monthly SEDI series calculated using the remaining six probability distributions for which the null hypothesis of normality was rejected (fail-to-reject rate) by the SW test at a confidence level $p = 0.05$.

	Log-logistic		GEV		Pearson III		Generalized Pareto		Normal		Exponential	
Month	GLEAM	CRU	GLEAM	CRU	GLEAM	CRU	GLEAM	CRU	GLEAM	CRU	GLEAM	CRU
Jan	75.9	60.0	68.0	58.6	65.7	58.2	20.4	13.1	35.5	46.6	11.2	8.2
Feb	74.3	57.6	68.7	57.1	66.6	56.7	22.4	14.7	38.8	46.7	10.7	8.8
Mar	86.3	66.3	79.4	64.4	77.0	65.2	24.0	14.3	50.3	53.4	14.4	9.2
Apr	89.0	78.1	81.3	74.2	79.3	74.6	22.6	15.4	51.3	59.3	16.1	10.2
May	91.4	88.7	83.2	85.5	80.8	86.1	23.6	18.0	51.3	71.5	15.2	12.0
Jun	92.8	89.1	81.6	85.5	79.9	86.3	19.5	18.9	48.2	71.9	11.8	12.0
Jul	91.4	88.9	80.8	84.9	78.5	86.2	19.1	18.5	44.2	71.3	10.6	11.1
Aug	87.7	88.8	75.8	85.1	72.1	86.0	17.9	17.7	36.5	68.1	11.2	11.0
Sep	87.3	88.7	73.9	85.4	70.7	86.0	20.4	17.9	36.6	71.5	12.3	11.7
Oct	83.6	72.3	72.8	70.8	70.2	70.6	19.2	17.9	38.1	58.0	12.5	11.1
Nov	81.8	59.0	73.3	56.8	71.1	56.5	20.1	11.9	40.9	46.5	12.8	7.4
Dec	76.9	53.4	68.2	52.4	66.4	51.8	18.3	12.6	37.7	40.2	10.8	7.6

relationship between vegetation activity and drought is strongly dependent on the drought time scale (Vicente-Serrano et al. 2013), the correlation between the sNDVI and the SPEI was calculated at time scales ranging between 1 and 24 months. Given the strong seasonality of vegetation, correlations were calculated independently for specific months of the year as well as for the monthly time series as a whole. Regardless of the time scale of the SPEI, we only retained the lag of maximum correlations and compared it spatially with the correlations obtained between sNDVI and SEDI.

4. Results

a. *Assessment of probability distributions to calculate the SEDI at the global scale*

Table 1 shows the percentage of monthly series for which the SEDI could not be calculated based on GLEAM and CRU TS AED data for each of the eight probability distributions used for standardization. The lognormal and Weibull distributions showed a markedly high percentage of series (often exceeding 40% of the terrestrial land surface) with no solution for the SEDI, suggesting that they are least suited for SEDI calculation, so they were removed from further analyses. The remaining six distributions showed smaller percentages of cases for which no solution could be found, with normal and exponential distributions being slightly better. Interestingly, there is a clear seasonal pattern in the ability of these six distributions to fit the ED series, with better performance found between March and September, compared to the October–February period. In comparison to the GLEAM AED, the SEDI calculated using the CRU TS AED shows a lower percentage of cases with no solution for the SEDI fitting. This may be explained by the higher AED values found in the CRU TS dataset.

The Shapiro–Wilks normality test applied to the SEDI series computed using the six remaining distributions indicated a poor performance of the generalized Pareto, normal, and exponential distributions, which had large percentages (typically 50%–90%) of monthly series for which the null hypothesis of normality was rejected (Table 2, for the GLEAM and CRU TS AED datasets, respectively). The remaining three distributions had a lower percentage of rejections, with the log-logistic distribution having the lowest overall. The results were similar with the two AED datasets considered, although the SEDI calculated with the CRU TS AED yielded worse results (i.e., a larger proportion of rejections). In both AED cases, there was a notable seasonality, with fewer rejections in the boreal summer (less than 10% for log-logistic) and more in boreal winter (around 25%).

Dry events are located in the lower tail of distribution, and it is important to discern departures from normality in this region, even though data located there may represent less than 2%–3% of all data. Figure 1a shows the relationship between the return periods and raw SEDI values obtained from GLEAM AED using log-logistic and GEV distributions, with Fig. 1b documenting similar for the log-logistic and Pearson-III distributions. The SEDI values obtained with GEV and Pearson-III distributions show more extreme values in both tails than those obtained with the log-logistic distribution. This translates to higher return periods and more extreme SEDI values with GEV and Pearson-III distributions in comparison to the log-logistic distribution.

The frequencies of high and low SEDI events using the GEV probability distribution for standardization are unrealistically high using a sample of 35 yr The plots

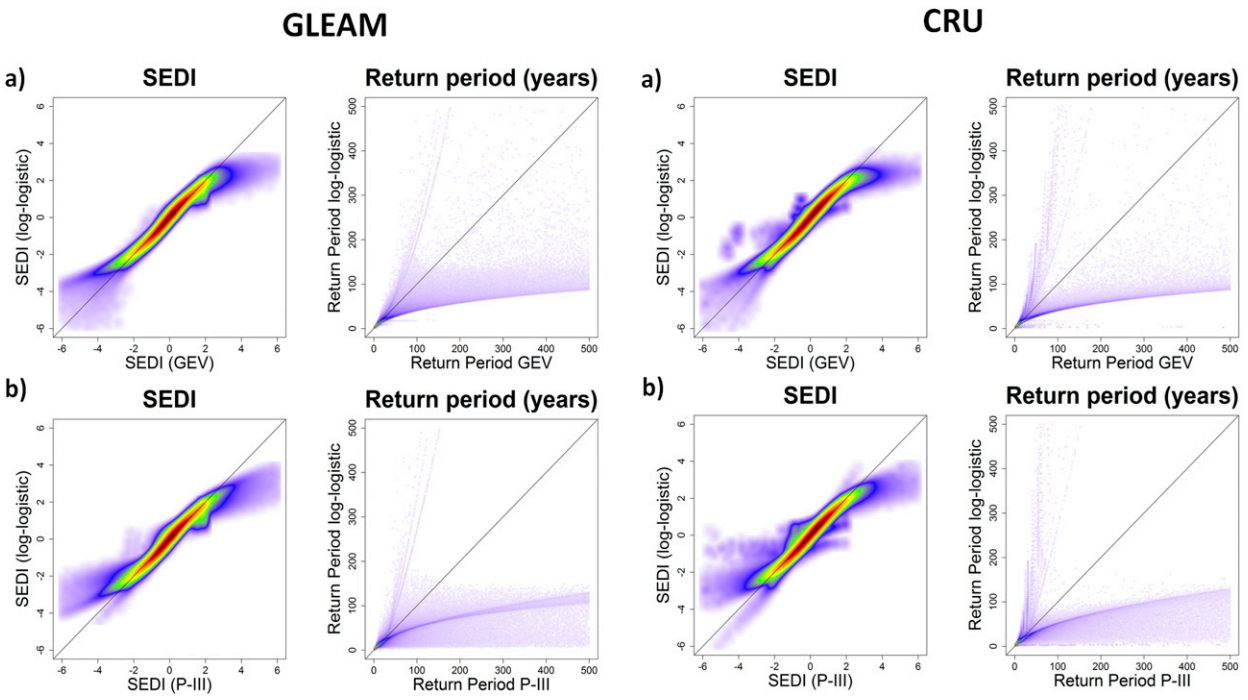

FIG. 1. Global terrestrial relationship between SEDI (and return period: 1 event in number of cases) obtained from (a) GEV and (b) Pearson-III distributions and log-logistic distribution using the (left) GLEAM and (right) CRU TS AED. Colors represent the density of points (dark red is the highest density).

are truncated to 1 event in 500 cases, corresponding to $\pm 2.88\sigma$, but even longer return periods were obtained with the GEV. On the other hand, the log-logistic distribution provided more coherent return periods and less extreme SEDI values. The plots also show that differences found in the high-density region ($\pm 1.80\sigma$) between the different probability distributions have only a residual influence on the SEDI values. The results based on the CRU TS AED yielded similar results. This is clearly illustrated in Fig. 2, which shows the frequency of values below -2.58σ (which corresponds to a return period of 1 in 200 yr) in each time series. As expected, the majority of series do not show values below the threshold, but lower percentages dominate for the log-logistic distribution. The SEDI series obtained with GEV and Pearson III distributions show higher percentage of very extreme values. Given the relatively short sample used here (1980–2014, with the start date determined by when the satellite remote sensing first becomes available), it is unlikely to find such a high frequency of SEDI cases corresponding to a return period higher than 200 years. Considering these results altogether (i.e., Tables 1 and 2 and Figs. 1 and 2), we recommend the use of the

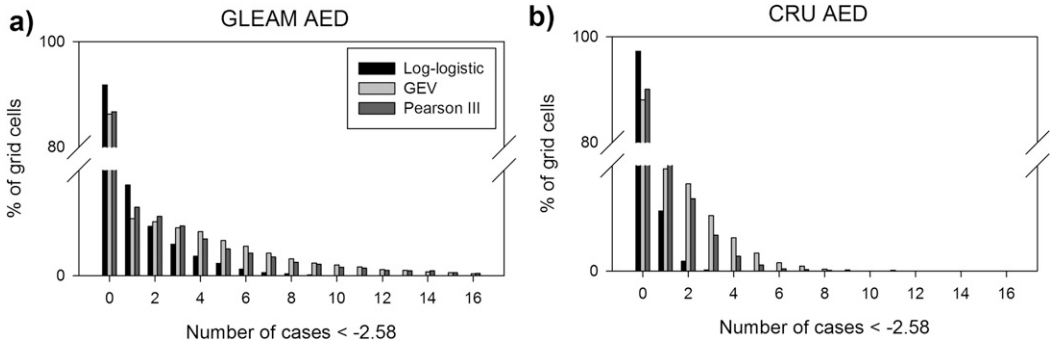

FIG. 2. Percentage of series showing absolute frequencies of SEDI values below -2.58σ: (a) GLEAM and (b) CRU TS AED.

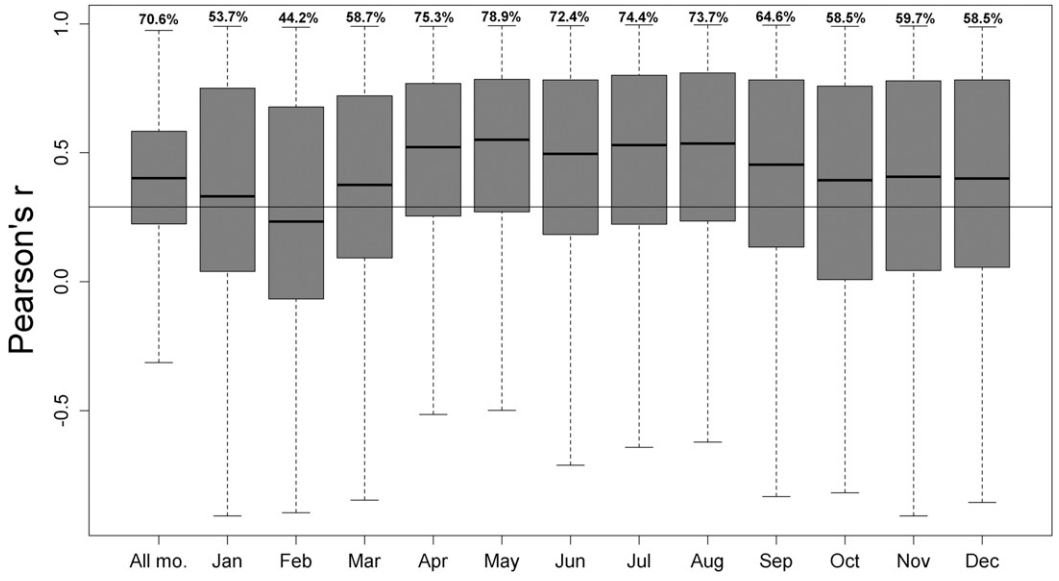

FIG. 3. Box-and-whisker plots showing the r between SEDI series calculated from GLEAM and CRU TS AED for the entire monthly record and for each month independently. The thin horizontal line shows the threshold for positive and significant correlations ($p < 0.05$), with numbers above the top whisker indicating the percentage of global terrestrial area with such correlations. The thick line in the box represents the median, the upper and lower parts of the box denote the interquartile range, and the whiskers show the 95% and 5% confidence levels.

log-logistic distribution for computing the SEDI series across the globe.

b. *Comparison of SEDI series from two different AED datasets*

The box-and-whisker plots in Fig. 3 summarize the per-pixel correlations between the SEDI series and the GLEAM and CRU TS AED datasets. All calculations were computed independently for each month for the 34 years, and for the entire monthly time series altogether. In general, correlations were dominantly positive and statistically significant ($p < 0.05$), albeit being generally higher for April and September inclusive. There is large variability in the box-and-whisker plots, especially during the Northern Hemisphere cold season where Pearson correlation coefficient r ranges from maximum positive to maximum negative values. Nevertheless, with the exception of the Northern Hemisphere cold season, the percentage of series showing significant correlations across the globe was generally higher than 70%. Figure 4 depicts the spatial distribution of correlations between both datasets annually and for the midseason months (i.e., January, April, July, and October). Results reveal markedly seasonal differences. During the boreal winter (i.e., January), large areas of the Northern Hemisphere were not considered, given that the SEDI had no solution for this region in the majority of the cases, as discussed in section 3. Nevertheless, in low latitudes, there were noticeable spatial differences in the correlations. Although the latter were high in the majority of tropical and subtropical regions, they were close to zero in the equatorial humid regions. This pattern persists in all seasons and all months. Overall, during the boreal spring (i.e., April) and summer (i.e., July), large regions showed statistically significant correlations between the SEDI calculated using AED from CRU TS and GLEAM.

The analysis of selected drought events illustrates a good agreement between the two datasets. Figure 5 shows two recent exceptional droughts: 1) Russia (2010; Fig. 5, top) and 2) southern United States and northern Mexico (2011; Fig. 5, bottom). In both events, although there are some spatial differences in the beginning and end of the drought periods, strong spatial agreement was exhibited between the two SEDI datasets during the months of maximum extension of drought severity (July and August for Russia and June–August for southern North America).

c. *Comparison of the SEDI and the SPEI at different time scales*

To avoid redundancy in the presentation of the results, in the following we only use the SEDI series obtained with the GLEAM AED dataset and the log-logistic standardization. The temporal variability of the SEDI showed a strong agreement with the SPEI. Considering only the SPEI time scale with the best correlation with the SEDI,

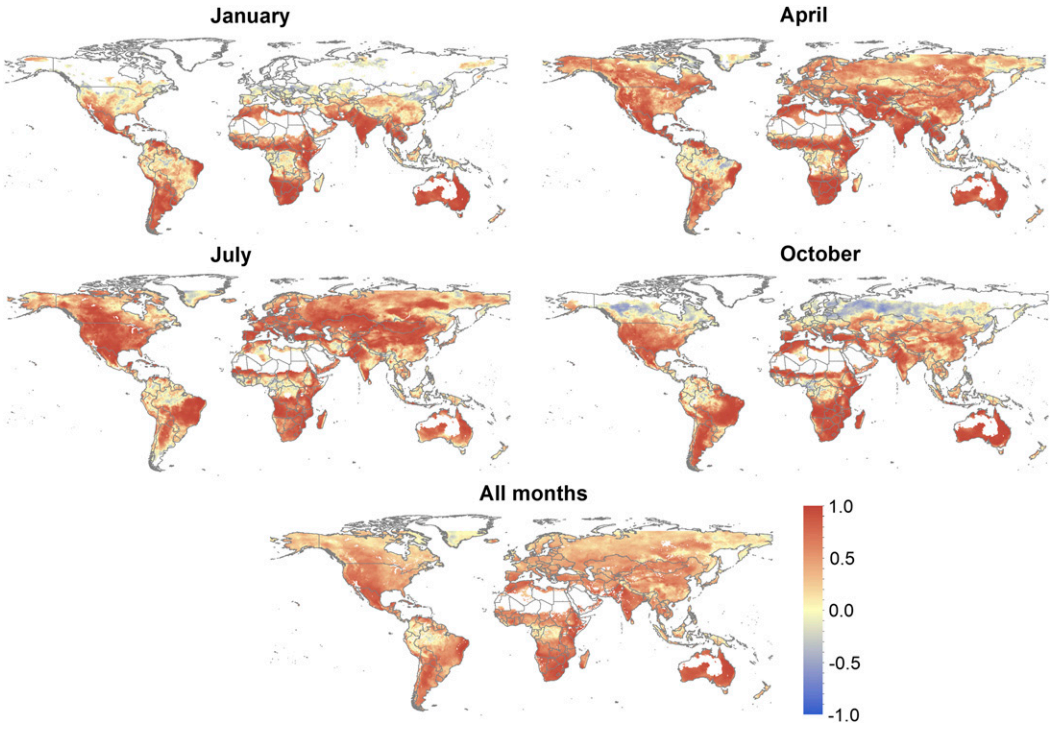

FIG. 4. Spatial distribution of the correlations between SEDI series calculated using the GLEAM and the CRU TS datasets for AED for the midseason monthly series and for the series of all months. Terrestrially white areas represent deserts and Greenland and areas in which the SEDI fit has no solution.

large areas exhibited significant correlation ($p < 0.05$) between both indices (Fig. 6). For instance, in the boreal summer, more than 85% of the world exhibited significant correlations between the SEDI and SPEI, despite the exceptionally low correlation in the rain forests of Amazonia, Congo, and Southeast Asia (Fig. 7). In general, the globe's semiarid regions showed the strongest (typically >0.7) significant correlations between both drought indices, likely reflecting the ample seasonal cycle and multiannual climate variability in these regions.

SEDI series exhibited higher correlations with short SPEI time scales (Fig. 8). Independent of the month, correlations were significant ($p < 0.05$) over the majority of the globe, considering SPEI time scales between 1 and 9 months. With respect to longer time scales, the magnitude and statistical significance of the correlations diminished progressively. In the boreal summer, the differences in the magnitude of the correlations among the different time scales were lower, but lower correlations were observed for long SPEI time scales. About 40% of the world exhibited the strongest correlation at the 1-month SPEI time scale, compared to 15%–20% at the 2-month time scale (Table 3). In summary, around 80% of world exhibited the highest and most statistically significant ($p < 0.05$) correlations between the SEDI and SPEI considering SPEI time scales shorter than 5 months. Exceptionally, a few regions (<10% of the terrestrial globe) showed the highest and most significant correlations at time scales longer than 9 months. Thus, during the boreal winter, apart from some areas in South America and central Africa and in northern latitudinal areas, the majority of regions showed maximum correlation between the SEDI and SPEI at short SPEI time scales (Fig. 9). The areas that did not show significant correlations between the SEDI and SPEI mostly corresponded to those showing higher correlations at longer time scales (>12 months). This finding demonstrates that where the SEDI is significantly correlated with SPEI, this correlation is recorded at short SPEI time scales (>5 months).

d. Relationships among the SEDI, SPEI, and the sNDVI

Figure 10 illustrates the spatial distribution of the correlations between the SEDI and sNDVI and between SPEI and sNDVI for midseason months and for the entire record. There were important spatial differences in the magnitude of the correlations between the sNDVI and both drought indices at the global scale. Regardless of the month, higher and statistically significant correlations

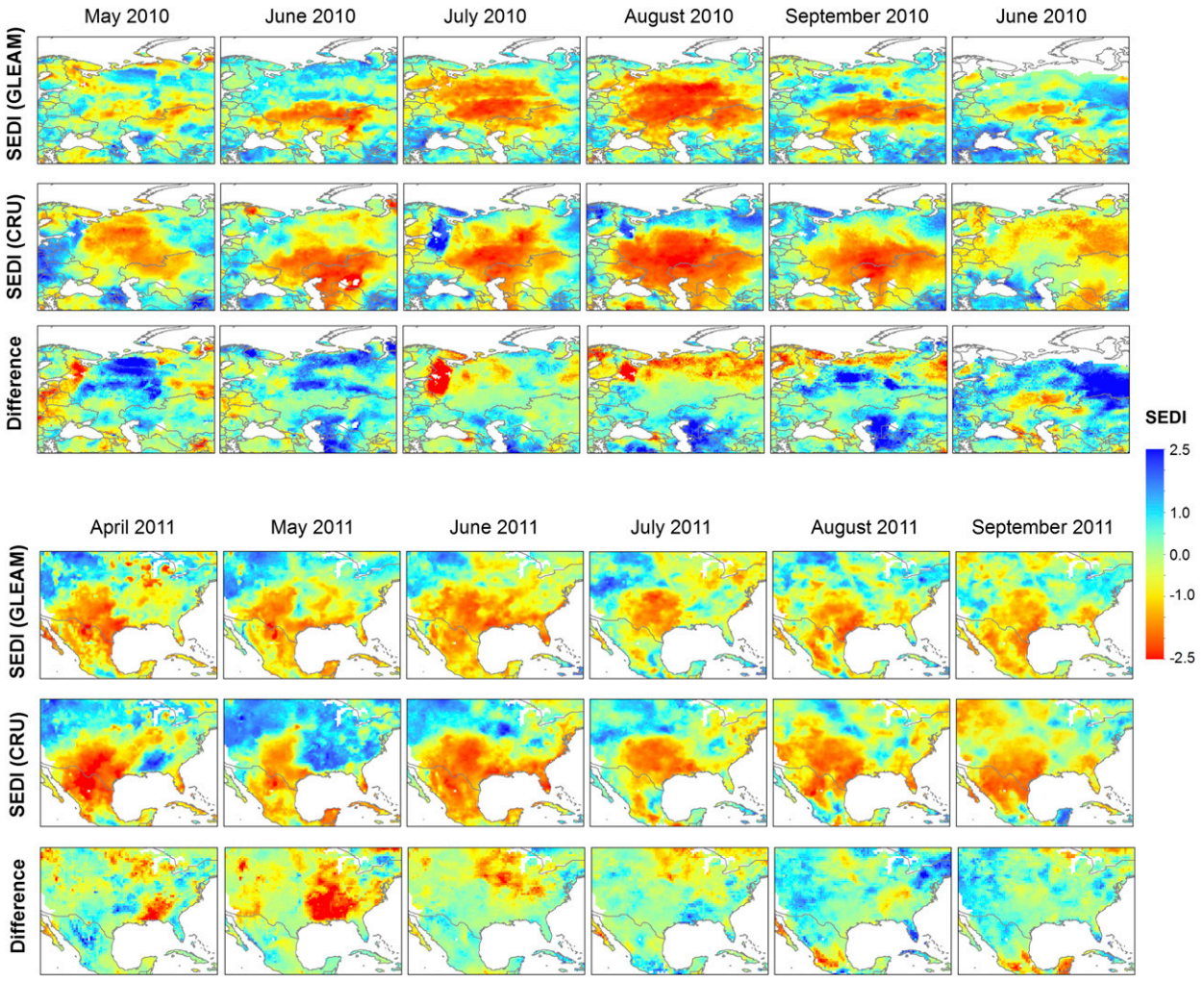

FIG. 5. Spatial distribution of the SEDI values obtained from GLEAM and CRU TS AED data during the recent drought episodes that affected (top) Russia and (bottom) southern North America in 2010 and 2011, respectively.

were found over semiarid regions, including southwestern North America, the Sahel, South Africa, Australia, and northeastern Brazil, among others. Strong seasonality in the correlations related to the phenological cycles of vegetation was found. Monthly cross plots of SEDI and SPEI and their correlations with sNDVI are seen Fig. 11, which illustrates that the spatial correlations were positive and statistically significant during all months. The correlations with sNDVI were higher for SPEI than for SEDI, particularly in the boreal summer (i.e., JJA).

The percentage of the terrestrial globe that showed significant correlations between either SEDI and sNDVI or SPEI and sNDVI were relatively small (typically ~15%–45%; see Table 4). For the full monthly time series, less than 20% of the area exhibited significant correlations, independent of the selected drought index. This low percentage is partly explained by the fact that most ecosystems on Earth are not driven by water availability during one or more periods of the year (e.g., dormancy). Monthly correlations between the sNDVI and SPEI were statistically significant over more than 40% of the area during the boreal summer, where vegetation is active in large areas of the Northern Hemisphere. The SEDI showed lower percentages, with roughly 25% of the area showing significant correlations with the sNDVI during the same season.

5. Discussion

a. Data used in the computation of the drought index

In this study we delve into the computation and performance of the SEDI. The SEDI is based on the ED, which is defined as the difference between the ETa and

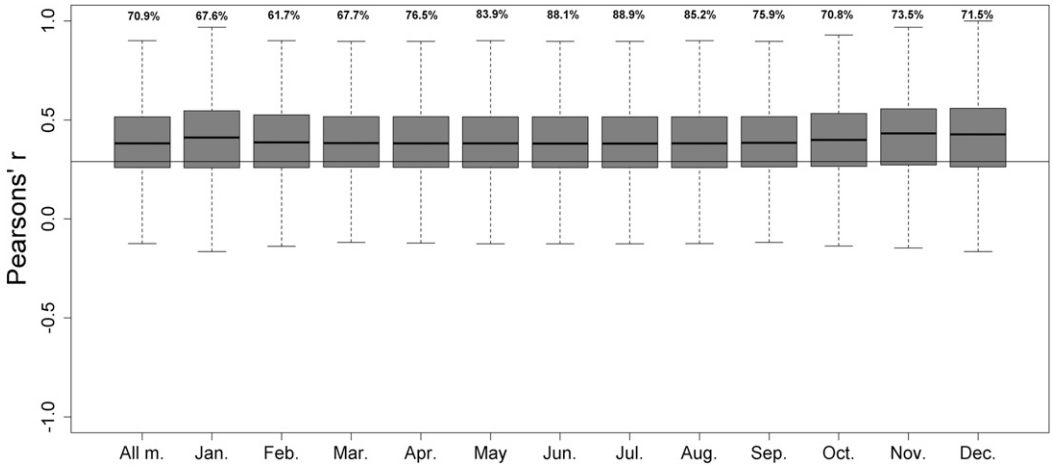

FIG. 6. Box-and-whisker plots showing r between the SEDI and SPEI for specific months of the year as well as for the entire record. The thin horizontal line shows the threshold for positive and significant correlations ($p < 0.05$), with numbers above the top whisker indicating the percentage of global terrestrial area with such correlations. The thick line in the box represents the median, the upper and lower parts of the box denote the interquartile range, and the whiskers show the 95% and 5% confidence levels.

the AED. The rationale behind this computation is to explicitly account for the water actually used by the vegetation (the ETa) compared with the amount of water that the same ecosystem would have used in an ideal perfect hydric state (i.e., with no water stress). The departures between ETa and AED allow quantification of the degree of water stress the vegetation is suffering (i.e., the drought state). Nevertheless, it is also necessary to state that ED defined here may depend on many other factors (e.g., leaf-out period, harvesting, fire, and pests) and not just water availability.

A major technical problem with this approach is how to obtain values of both ETa and AED, most notably the former. The recent availability of global ETa datasets based on satellite observations (McCabe et al. 2016; Miralles et al. 2016; Zhang et al. 2016), however, has opened the possibility to explore this approach.

Several studies have already proposed the quantification of drought severity based on either the ED or the ratio between ETa and AED, or by using ETa estimations obtained from remote sensing data (e.g., Yao et al. 2010; Anderson et al. 2011). In their South Korean study, Kim and Rhee (2016) proposed the use of the ED to develop a drought index. They estimated ETa following the Budyko theoretical approach, which establishes a nonlinear relationship between the AED–precipitation ratio and the ETa–precipitation ratio. The novelty of our study is that it calculates the SEDI globally, using ETa from a global satellite dataset (GLEAM). Despite the uncertainties in GLEAM, its detailed description of the soil water balance and phenological stress mean an improvement over using ETa estimations using Budyko's hydroclimatic framework (Martens et al. 2017).

Regarding the AED data, two datasets were compared to calculate the SEDI globally. The first (GLEAM) calculates AED using the Priestley and Taylor's (1972) ETp formulation (Priestley–Taylor scheme). The second (CRU TS) calculates AED using a simplification of Allen et al.'s (1998) FAO-56 Penman–Monteith equation. Several studies have shown that the spatial and temporal variability of the AED is strongly dependent on the methodology used to estimate this variable (e.g., Espadafor et al. 2011; Vicente-Serrano et al. 2014; Wang et al. 2015; Fisher et al. 2011) and on the uncertainty in the atmospheric forcing data (McVicar et al. 2012a,b). Here, we assessed the sensitivity of the global-scale SEDI to the choice of AED and found notable differences in the boreal winter months (i.e., DJF) and also in the humid equatorial regions during their summer months (i.e., JJA); these are regions in which the aerodynamic component of AED can be substantial (McVicar et al. 2012b). As the Priestley–Taylor scheme is a radiative-based estimate of ETp (Donohue et al. 2010) that does not include aerodynamic variables (i.e., relative humidity) explicitly in its calculations, whereas the FAO-56 Penman–Monteith formulation does, they are expected to depart. Conversely, in subhumid to semiarid climates of both hemispheres, and especially during their summer, the correlation between the two SEDI datasets was strong and not sensitive to the AED dataset used in the calculations. This is highly relevant for drought analysis and monitoring since in these regions vegetation

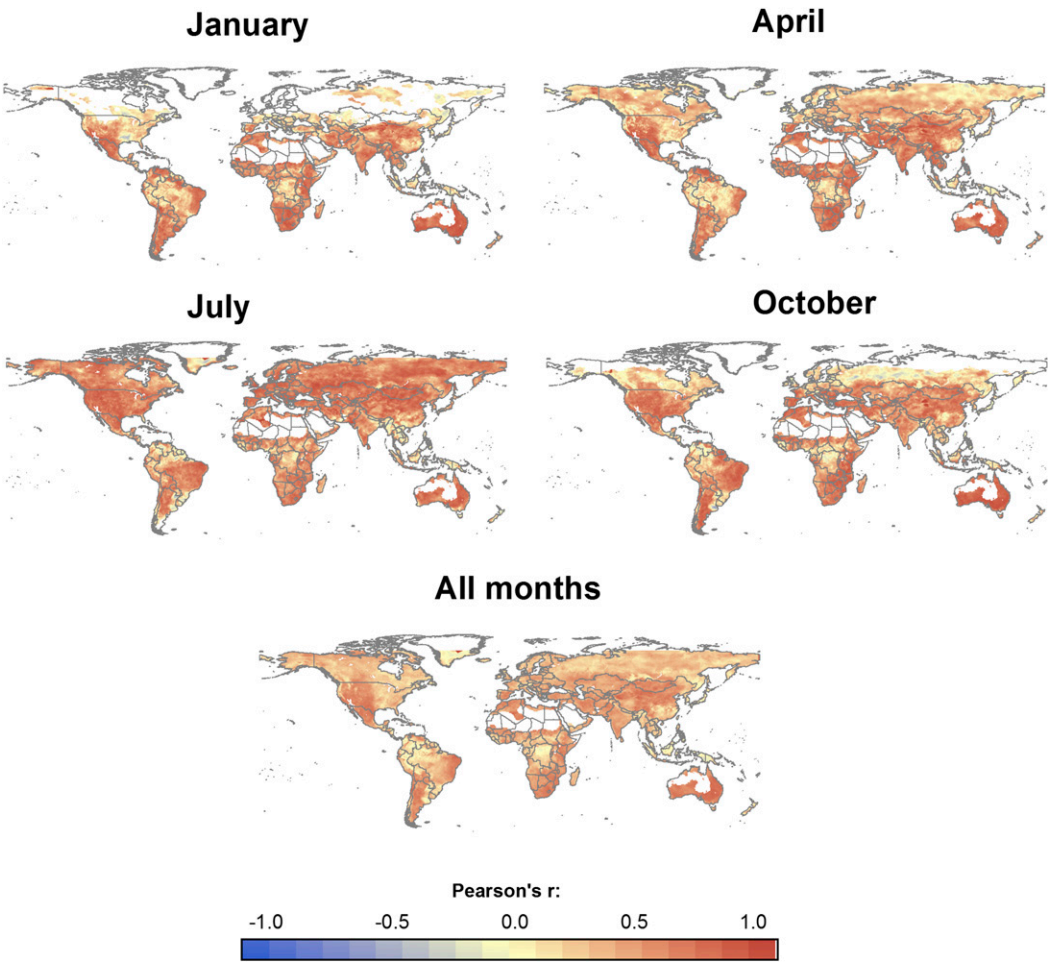

FIG. 7. Spatial distribution of the correlations between SEDI and SPEI series for midseason months and for the entire record. Terrestrially white areas represent deserts and Greenland and areas in which the SEDI fit has no solution.

dynamics are more determined by drought variability (Vicente-Serrano et al. 2013).

In tropical forests, the correlation between both SEDI datasets was statistically not significant, regardless of the season of the year. There are several factors driving this pattern. It can be related to the low climate data availability. While GLEAM AED uses reanalysis output the CRU TS AED depends on observational data, which are sparse over these regions (Harris et al. 2014). It can also be related to uncertainties in the reanalysis output meteorological fields, which are the likely cause for the difference found between the two SEDI datasets, particularly for those variables that are most difficult to model, such as wind speed and solar radiation (McVicar et al. 2008; Perdigao et al. 2016). Moreover, the lack of relative humidity in the Priestley–Taylor scheme could affect the estimations, given that strong changes in this variable have been recorded in observations and reanalysis output over the past two decades (Willett et al. 2014; Vicente-Serrano et al. 2017), and it is taken into account in the Penman–Monteith ETo.

Despite the differences found, the SEDI provides a quantification of the intensity of drought that is largely independent of the method used to compute the AED in most global regions affected by recurrent droughts events. Low sensitivity of the SEDI to the methodology used to estimate AED is relevant for the evaluation of impact in some regions such as the Sahel, South America, or central Asia. In these regions the impacts of droughts are usually severe, and quantifying the extent and intensity of drought conditions is critical to inform policy and guide mitigating action.

Although we provide an initial assessment of the impact of using different datasets to compute the SEDI at globally, further research is needed to test

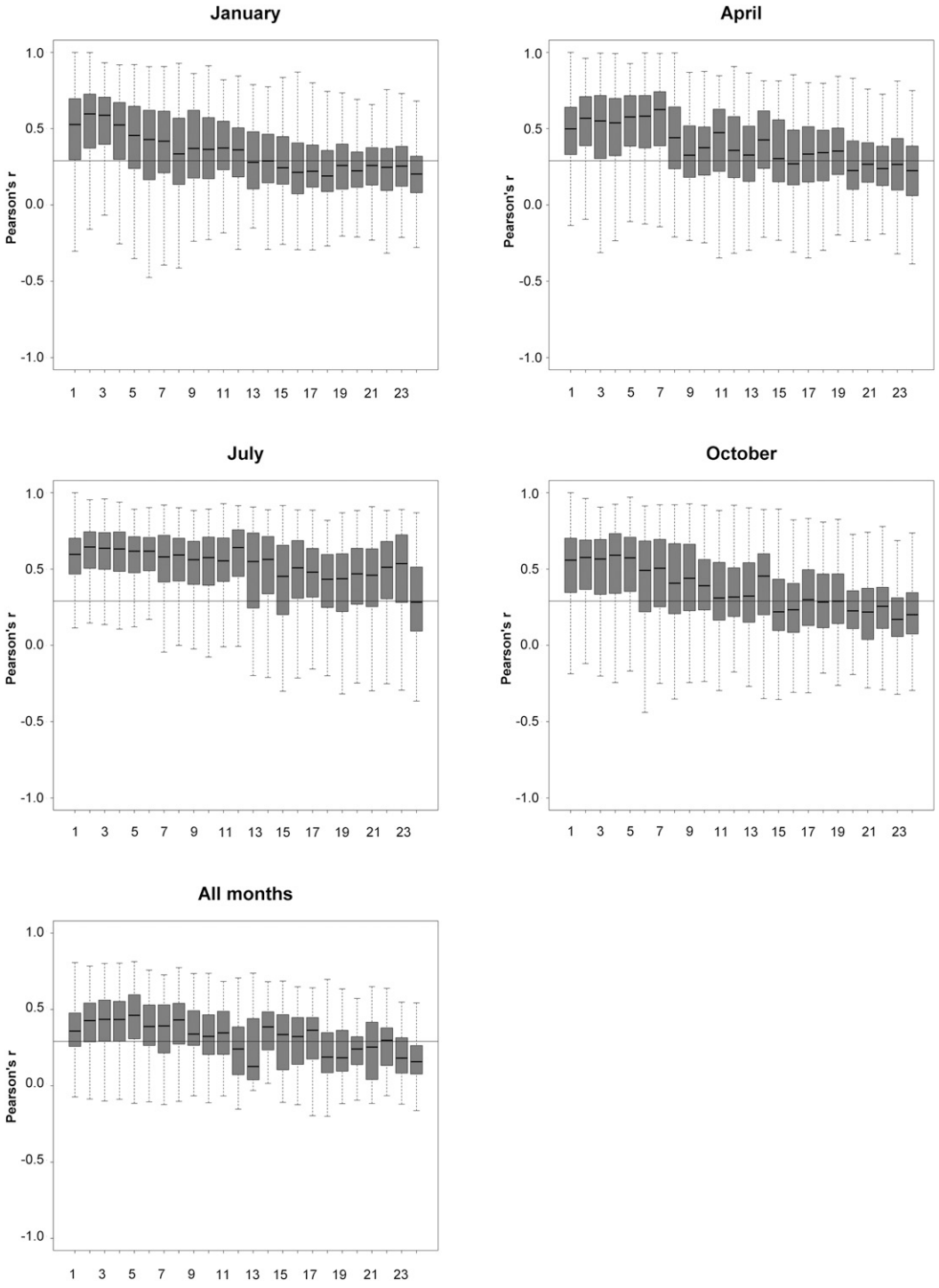

FIG. 8. Correlation between the SEDI and SPEI at different time scales (from 1 to 24 months) for specific months and for the entire record. The thin horizontal line shows the threshold for positive and significant correlations ($p < 0.05$), with numbers above the top whisker indicating the percentage of global terrestrial area with such correlations. The thick line in the box represents the median, the upper and lower parts of the box denote the interquartile range, and the whiskers show the 95% and 5% confidence levels.

TABLE 3. Percentage of global terrestrial 0.5° resolution grid points at which the maximum correlation between the SEDI and SPEI is recorded corresponding to different SPEI time scales.

SPEI time scale (month)	All months	Jan	Feb	Mar	Apr	May	Jun	Jul	Aug	Sep	Oct	Nov	Dec
1	42.0	21.5	24.5	31.9	40.7	42.0	42.0	38.0	32.9	33.5	23.4	24.5	20.2
2	20.2	14.9	13.5	14.6	14.3	14.7	13.9	17.6	17.9	14.9	17.1	19.2	17.8
3	9.7	11.9	8.2	10.1	8.5	8.3	9.4	7.6	9.8	9.6	9.3	12.1	13.1
4	7.5	7.8	8.6	6.7	6.6	4.5	6.0	6.4	6.9	7.1	7.8	5.8	7.5
5	4.3	5.2	5.3	5.1	4.5	4.2	3.6	4.5	4.7	4.3	6.3	4.9	5.8
6	3.7	4.8	4.6	5.1	2.7	3.2	3.0	3.5	3.6	3.6	4.1	4.2	4.0
7	2.3	3.1	4.2	3.8	3.0	3.1	2.4	2.6	2.3	2.7	2.9	3.3	3.4
8	1.9	3.5	2.9	2.8	2.4	2.8	2.7	2.3	1.8	1.8	2.5	3.6	2.7
9	1.3	2.1	4.4	2.6	1.8	2.4	2.2	2.1	1.7	1.4	1.5	1.8	3.4
10	1.1	2.0	2.5	1.4	2.2	2.7	2.4	1.8	1.7	1.9	1.9	1.7	2.5
11	0.7	1.6	2.0	1.5	1.6	1.5	1.6	2.3	1.6	1.7	1.2	1.6	1.7
12	0.5	1.5	1.2	1.5	1.3	1.1	1.3	1.8	2.7	1.9	1.3	1.5	1.2
13	0.3	1.1	0.8	0.8	0.8	0.8	0.8	0.8	1.5	1.3	1.4	0.9	1.0
14	0.2	1.1	0.9	0.6	0.6	0.5	0.8	0.9	1.6	1.9	1.6	1.0	1.0
15	0.3	1.3	1.2	0.8	0.5	0.4	0.8	0.7	1.3	1.6	1.7	1.3	1.2
16	0.3	2.0	1.3	0.8	0.6	0.5	0.5	0.7	0.8	1.2	2.1	1.0	1.0
17	0.3	1.5	1.0	0.6	0.6	0.5	0.6	0.5	0.7	1.0	2.1	1.5	1.2
18	0.1	1.9	1.0	0.9	0.6	0.5	0.6	0.5	0.6	0.9	1.1	1.6	1.6
19	0.4	1.4	2.2	0.7	0.7	0.5	0.7	0.5	0.4	0.6	1.0	1.1	1.6
20	0.5	1.5	1.6	1.1	1.2	0.8	0.6	0.7	0.6	0.5	1.0	1.3	1.3
21	0.4	1.9	1.8	1.6	0.9	1.1	0.6	0.6	0.8	1.0	0.7	1.0	1.4
22	0.4	1.6	1.7	1.4	0.6	0.8	0.9	0.7	0.7	1.1	1.4	1.1	1.2
23	0.5	1.5	1.4	1.1	1.0	1.2	1.1	1.0	1.1	1.6	2.9	1.2	1.7
24	1.3	3.7	3.0	2.8	2.3	1.8	1.6	2.1	2.5	2.8	3.7	2.9	2.8

the sensibility of the SEDI to both ETa and AED variables under a range of climate and land-cover conditions and to investigate the impact of using different ETa and AED datasets in the calculation of the SEDI. Meanwhile, there are several international initiatives to improve the quality and assess the uncertainties in global ET data from satellite and in situ observations (Zhang et al. 2016; McCabe et al. 2017; Fisher et al. 2017).

b. *Optimum probability distribution to calculate the SEDI worldwide*

This study tested eight standardized probability distribution approaches to calculate the SEDI and proposed a robust methodology to obtain global SEDI values that are spatially and temporally comparable. The log-logistic probability distribution showed clear advantages for calculating the SEDI. This distribution has already been recommended when calculating the SPEI (Vicente-Serrano et al. 2010a; Vicente-Serrano and Beguería 2016). From the tested distributions, only the GEV, Pearson-III, and log-logistic distributions provided solutions for the SEDI over most of the terrestrial globe and provided SEDI series that most frequently followed a standard normal distribution. The Pearson-III distribution has been proposed to calculate the SPI (Guttman 1999; Vicente-Serrano 2006) as the most reliable alternative to the original proposed standardization using the gamma distribution (McKee et al. 1993). However, here we found that the Pearson-III distribution yielded a higher number of SEDI series that did not follow a normal distribution compared to the log-logistic distribution. Moreover, the Pearson-III distribution tended to overestimate the frequency of extreme SEDI values at both ends of the distribution. The same was found with the GEV distribution, proposed by Stagge et al. (2015) for calculating the SPEI. Based on our global results, we recommend the use of the log-logistic distribution to fit monthly ED series across the terrestrial environment to obtain the SEDI. Moreover, this recommendation holds independently of the AED form used in this study.

c. *Comparison of the SEDI with the SPEI*

The SPEI has been thoroughly validated and used to detect and monitor moisture anomalies for agricultural (e.g., Zipper et al. 2016; Wang et al. 2006; Páscoa et al. 2017) and environmental applications (e.g., Zhang et al. 2017; Greenwood et al. 2017). The SEDI showed positive significant correlations with the SPEI over most terrestrial ecosystems, with some exceptions in the equatorial region and across some boreal regions. Under abundant soil moisture the SPEI could also show a

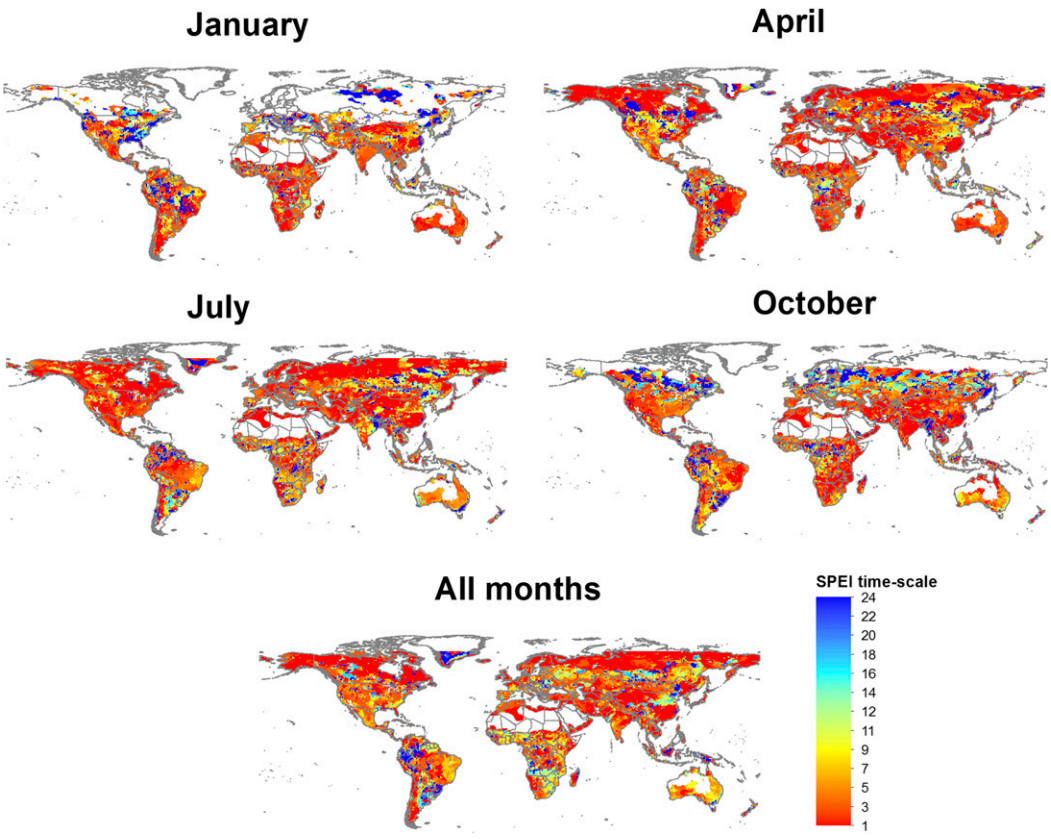

FIG. 9. SPEI time scale at which the highest correlation with the SEDI series was found for midseason months and for the entire record. Terrestrially white areas represent deserts and Greenland and areas in which the SEDI fit has no solution.

drought signal if precipitation is below average when really there is a limited plant available soil water constraint. This suggests that in some areas SPEI and SEDI are complementary. In areas in which the ETa strongly depends on precipitation (e.g., arid and semiarid regions), SPEI and SEDI are expected to fit well; in other regions they could provide different but complementary information to assess drought severity. Nonetheless, during the summer boreal season, the SEDI showed significant correlation with the SPEI over the entire Northern Hemisphere. If all data were perfect, SEDI would be better in capturing vegetation impacts simply because the use of precipitation in SPEI is meant to be as a surrogate for plant water availability. Thus, SPEI uses precipitation as proxy of ETa to identify drought impacts on vegetation. This approach, although less consistent physically than the SEDI, may produce better results to determine drought severity than a complex physical simulation model (i.e., Vicente-Serrano et al. 2011).

The SEDI was best correlated with the SPEI at short time scales, with the highest and most significant correlations recorded at 1- and 2-month time scales, independent of the month. There are a few regions where the strongest correlations between the SPEI and SEDI were observed at time scales longer than 18 months, but these correlations were not statistically significant. Therefore, we can regard SEDI as a short-time-scale drought index, characterized by its sensitivity to high-frequency climate variations. Kim and Rhee (2016) suggested the calculation of the SEDI at a time scale of 9 months by standardizing the cumulative ET and AED differences over the previous nine months. They justified the selection of this period by the high correlation found between the Palmer drought severity index (PDSI) and the SPEI at this time scale (see Vicente-Serrano et al. 2010b). We showed that in most regions of the world, the standardized anomalies of the ED are mostly determined by the high-frequency variability of the climatic water balance recorded at short time scales, which recommends the use of the SEDI at 1-month time scale.

The selection of a specific time scale for drought analysis is justified by the different characteristic

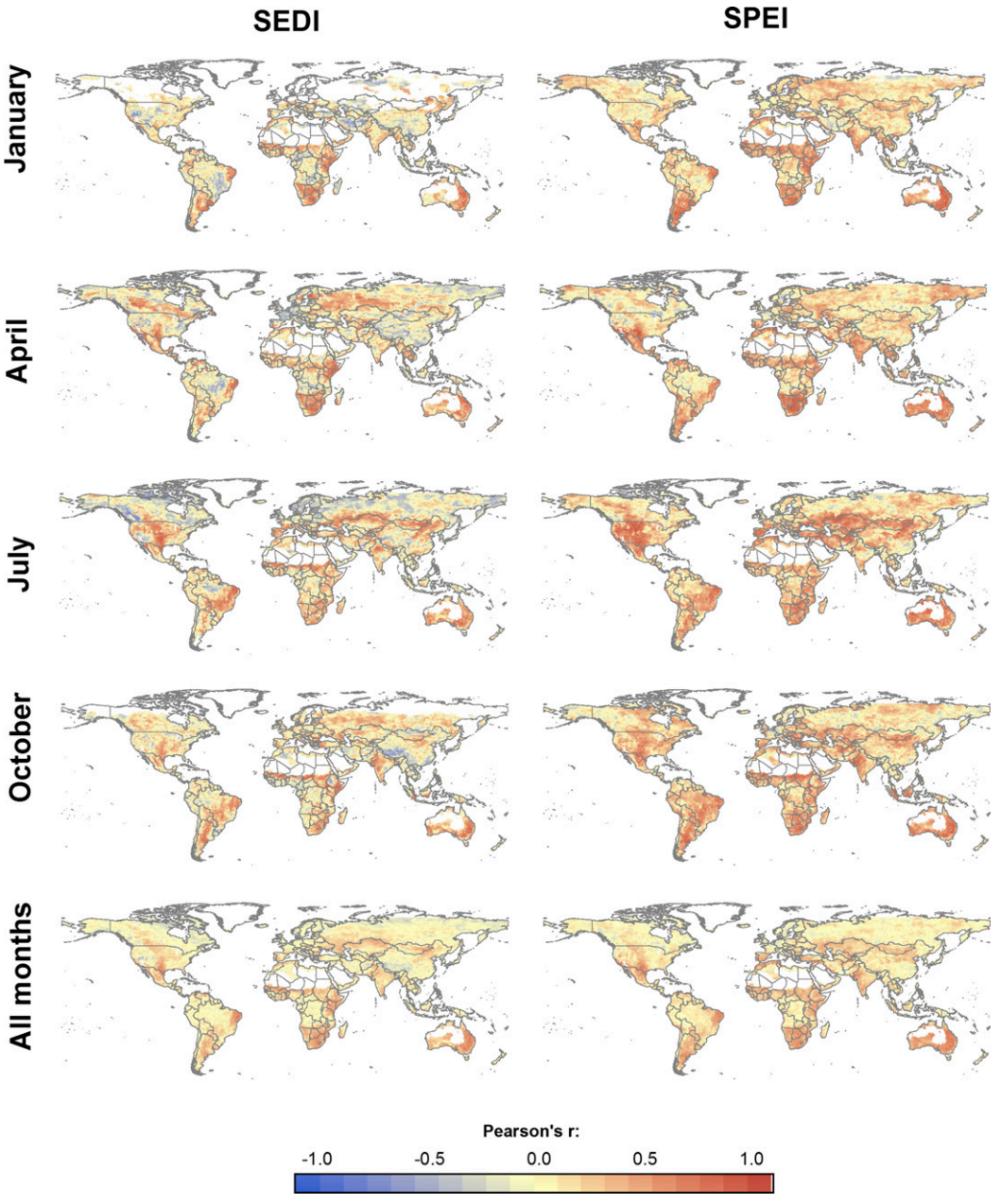

FIG. 10. Spatial distribution of the maximum r (left) between SEDI and sNDVI and (right) between SPEI and sNDVI for midseason months and for the entire record 1981–2014.

response times of agricultural, hydrological, and environmental systems to water shortage. Water shortages are mostly determined by precipitation shortfalls (McKee et al. 1993) and/or increased AED (Vicente-Serrano et al. 2010a). The use of different drought time scales is essential to adjust the duration of anomalous climate conditions to the anomalous response of the ecohydrologic system, such as abnormally low stream flows [e.g., López-Moreno et al. 2013; Lorenzo-Lacruz et al. 2013; Barker et al. 2016; see further clarifications and discussion on the drought time scales in Vicente-Serrano et al. (2011)]. However, the use of long cumulative time scales is not justified for the SEDI because ED is mostly determined by high-frequency variability in climatic conditions. In essence, this is similar to those streamflow-based drought indices, such as the standardized streamflow index (SSI) (Vicente-Serrano et al. 2012a). For instance, like the SSI, the SEDI could also

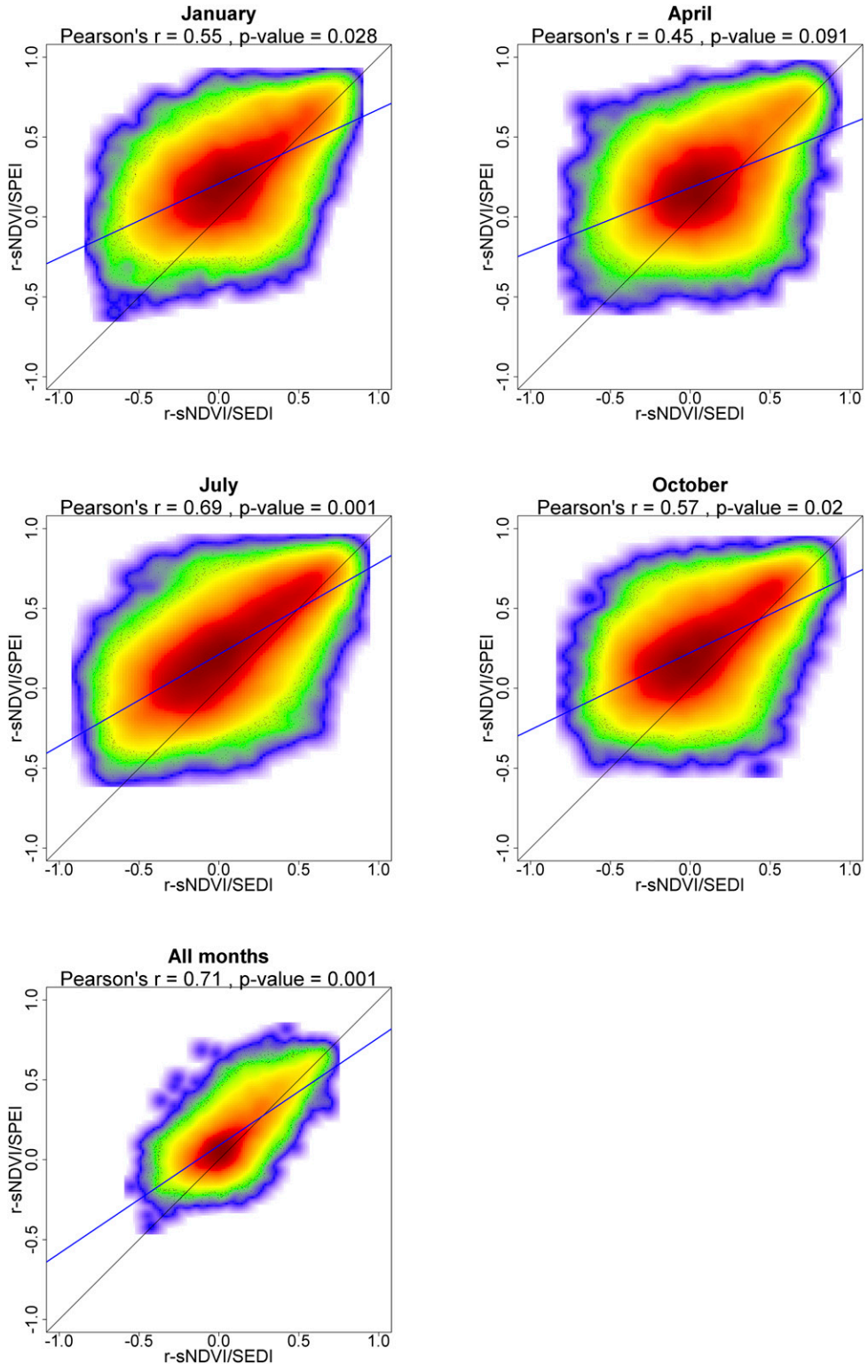

FIG. 11. Density scatterplots with the spatial relationship between the sNDVI and SEDI correlations and between the sNDVI and SPEI correlations. The scatterplots show the results for specific months and for the entire record. The blue line is a linear regression, and the black line is the 1:1 line. Given the large sample and to avoid an overrepresentation of significant correlations, the p values were obtained by means of a bootstrap sampling approach that considers 2000 independent samples of 30 cases, and p values for correlations of the samples of 30 cases were averaged. The colors of the scatterplots represent the density of points (dark red is the highest density).

TABLE 4. Percentage of the global terrestrial areas showing significant correlations between sNDVI and SEDI and between sNDVI and SPEI.

Month	sNDVI vs SEDI	sNDVI vs SPEI
All	13.09	19.24
Jan	23.52	36.94
Feb	22.74	35.68
Mar	23.59	37.12
Apr	26.67	38.08
May	27.81	37.63
Jun	24.49	41.22
Jul	26.84	43.88
Aug	26.21	46.72
Sep	23.95	43.67
Oct	25.35	42.92
Nov	25.41	37.64
Dec	28.93	39.10

be considered a direct indicator of the impact of droughts on vegetation because the AED is an important driver of vegetation gross primary production through its control on plant stomatal closure and plant respiration (Stephenson 1990, 1998) and because ETa strongly controls photosynthesis and carbon uptake (Donohue et al. 2014; Yang et al. 2015).

d. *Performance of the SEDI to identify vegetation anomalies associated with drought*

The response of vegetation activity, measured as greenness indices (e.g., NDVI) from satellite imagery, to water availability is complex. Numerous studies have demonstrated different spatial and seasonal relationships between NDVI and different climate drought indices (e.g., Ji and Peters 2003; Quiring and Paraprikaou 2003). Here, we demonstrated that the correlation between the sNDVI and the SPEI and SEDI was strongly variable over both space and time. As expected, a clear relationship was recorded in semiarid regions, which in general show a higher response to soil water availability, compared to subhumid and humid regions in which vegetation is driven by other climatic and environmental factors (Vicente-Serrano et al. 2013; Papagiannopoul et al. 2017). Overall, a lower correlation of the sNDVI to the SEDI than to the SPEI was found. In general, the correlations were higher and more frequently statistically significant between the sNDVI and SPEI, possibly due to the higher flexibility of the SPEI, which is computed at different time scales, since the relationship between vegetation activity and drought indices strongly differs as a function of the time scale at which drought indices were calculated (Pasho et al. 2011; Vicente-Serrano et al. 2013, 2015). SPEI would show higher flexibility to compute water deficits recorded at different time scales since vegetation types have several physiological strategies to cope with water stress (Chaves et al. 2003). Thus, stomatal closure under high vapor pressure deficit conditions is a mechanism to reduce water losses and hydrologic stress in plants. Although during periods of low transpiration photosynthesis may be reduced, nonstructural carbohydrates in the plant can maintain plant metabolism and maintain greenness (Rosas et al. 2013).

Overall, we indicated that although the SEDI showed lower correlations, it exhibited similar spatial patterns of correlation with the sNDVI. Compared to the SPEI, SEDI's sensitivity to high-frequency changes in ED makes it more suitable for identifying regions where leaf activity is highly sensitive to water stress conditions. We defend that using and combining different drought indices is the best approach for drought quantification, analysis, and monitoring. The recently proposed SEDI based on the satellite-based ET data can complement traditional drought indices and provide information about regions that are sensitive to short-term changes in atmospheric demand. Figure 12 provides a representative example of two exceptional drought events recorded in the Iberian Peninsula in 1995 and the Sahel in 1984. In both cases, the SEDI and 3-month SPEI showed strong drought severity over large areas and months, but they did not exactly agree either over space or in magnitude, which indicates that SEDI is bringing new information not captured by the SPEI. NDVI anomalies were different in time and space from each of the drought indices (SEDI and SPEI), indicating that none of them alone captures the full impact on vegetation greenness, with additional insight possible when both indices are combined.

6. Conclusions

We provided recommendations on the best approaches for calculating a temporally and spatially comparable SEDI, regardless of the climate region and land surface conditions. Although the SEDI is based on directly comparing the use of water (ETa) with its theoretical demand (AED), we have shown that other indices such as the SPEI that do not require estimation of the ETa showed a similar performance to identify drought severity globally. In any case, SEDI calculations will benefit from further improvements in remotely sensed ETa. Additionally, while the SEDI can be of interest for drought assessment related to crops and natural vegetation, its potential application in relation to other drought impacts such as river discharge, reservoir storage, or groundwater levels is yet to be explored. The SEDI global dataset developed in this study is available from Vicente-Serrano 2018.

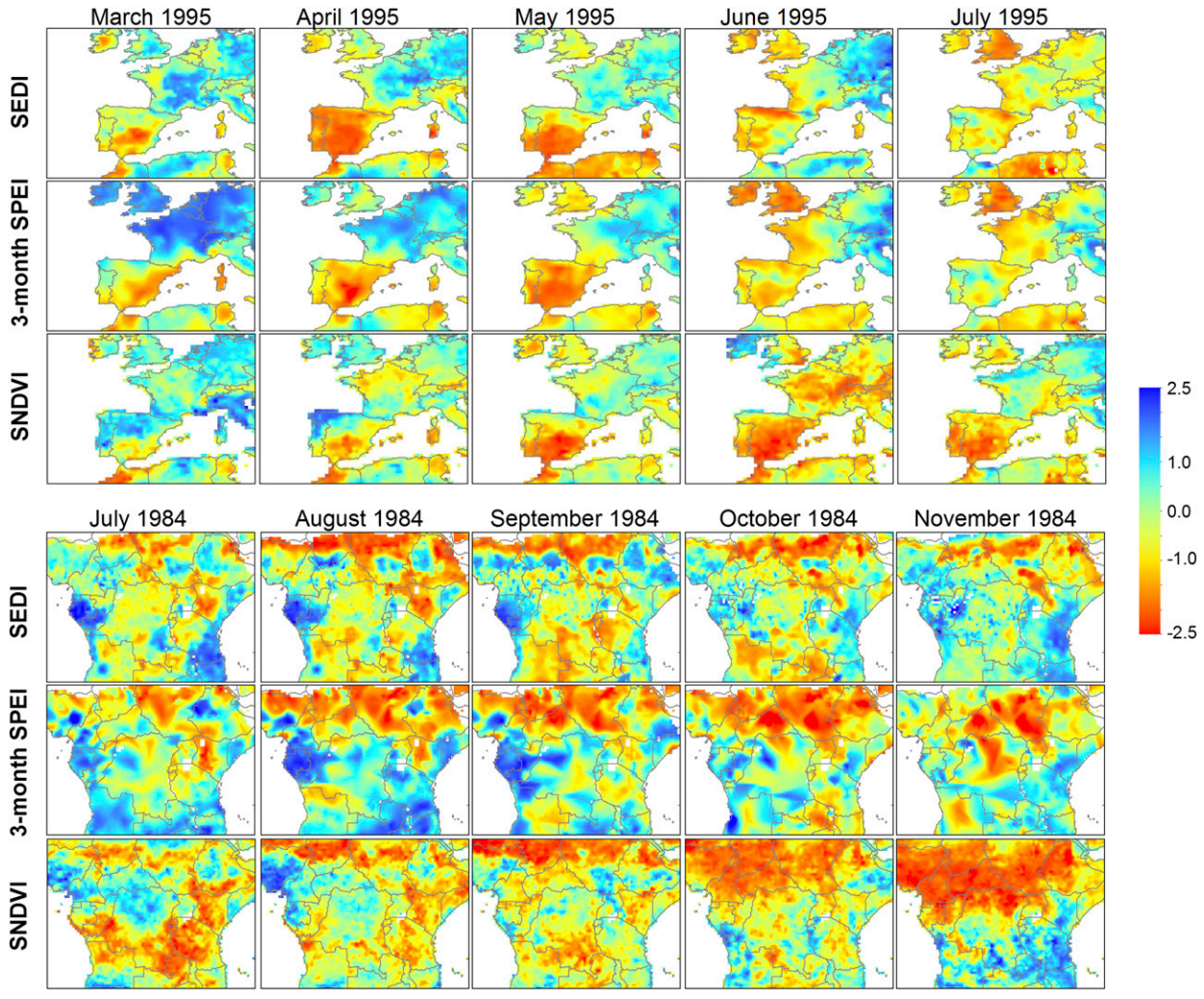

FIG. 12. Spatial distribution of the SEDI, 3-month SPEI, and sNDVI during two extraordinary drought events recorded (top) in 1995 over the Iberian Peninsula and (bottom) in 1984 over the Sahel.

Acknowledgments. This work was supported by the research projects PCIN-2015-220 and CGL2014-52135-C03-01 financed by the Spanish Commission of Science and Technology and FEDER. IMDROFLOOD financed by the Water Works 2014 co-funded all of the European Commission and INDECIS, which is part of ERA4CS, an ERA-NET initiated by JPI Climate, and funded by FORMAS (Sweden), DLR (Germany), BMWFW (Austria), IFD (Denmark), MINECO (Spain), and ANR (France), with co-funding by the European Union (Grant 690462). Diego G. Miralles acknowledges support from the European Research Council (ERC) under Grant Agreement 715254 (DRY–2–DRY). Marina Peña-Gallardo was supported by the Spanish Ministry of Economy and Competitiveness and Miquel Tomás-Burguera was supported by a doctoral grant by the Ministerio de Educación, Cultura y Deporte.

REFERENCES

Abramowitz, M., and I. A. Stegun, 1965: *Handbook of Mathematical Functions*. Dover Publications, 1046 pp.

Allen, C. D., D. D. Breshears, and N. G. McDowell, 2015: On underestimation of global vulnerability to tree mortality and forest die-off from hotter drought in the Anthropocene. *Ecosphere*, **6**, 129, https://doi.org/10.1890/ES15-00203.1.

Allen, R. G., L. S. Pereira, D. Raes, and M. Smith, 1998: Crop evapotranspiration: Guidelines for computing crop water requirements. Food and Agricultural Organization Irrigation and Drainage Paper 56, 300 pp., http://www.fao.org/docrep/X0490E/X0490E00.htm.

——, M. Tasumi, and R. Trezza, 2007: Satellite-based energy balance for mapping evapotranspiration with internalized calibration (METRIC)–Model. *J. Irrig. Drain. Eng.*, **133**, 380–394, https://doi.org/10.1061/(ASCE)0733-9437(2007)133:4(380).

Anderegg, L. D. L., W. R. L. Anderegg, J. Abatzoglou, A. M. Hausladen, and J. A. Berry, 2013: Drought characteristics' role in widespread aspen forest mortality across Colorado,

USA. *Global Change Biol.*, **19**, 1526–1537, https://doi.org/10.1111/gcb.12146.

Anderegg, W. R. L., A. Flint, C.-Y. Huang, L. Flint, J. A. Berry, F. W. Davis, J. S. Sperry, and C. B. Field, 2015: Tree mortality predicted from drought-induced vascular damage. *Nat. Geosci.*, **8**, 367–371, https://doi.org/10.1038/ngeo2400.

Anderson, M. C., C. Hain, B. Wardlow, A. Pimstein, J. R. Mecikalski, and W. P. Kustas, 2011: Evaluation of drought indices based on thermal remote sensing of evapotranspiration over the continental United States. *J. Climate*, **24**, 2025–2044, https://doi.org/10.1175/2010JCLI3812.1.

Antwi-Agyei, P., E. D. G. Fraser, A. J. Dougill, L. C. Stringer, and E. Simelton, 2012: Mapping the vulnerability of crop production to drought in Ghana using rainfall, yield and socioeconomic data. *Appl. Geogr.*, **32**, 324–334, https://doi.org/10.1016/j.apgeog.2011.06.010.

Asseng, S., and Coauthors, 2015: Rising temperatures reduce global wheat production. *Nat. Climate Change*, **5**, 143–147, https://doi.org/10.1038/nclimate2470.

Barker, L. J., J. Hannaford, A. Chiverton, and C. Svensson, 2016: From meteorological to hydrological drought using standardised indicators. *Hydrol. Earth Syst. Sci.*, **20**, 2483–2505, https://doi.org/10.5194/hess-20-2483-2016.

Beck, H. E., T. R. McVicar, A. I. J. M. van Dijk, J. Schellekens, R. A. M. de Jeu, and L. A. Bruijnzeel, 2011: Global evaluation of four AVHRR-NDVI data-sets: Intercomparison and assessment against Landsat imagery. *Remote Sens. Environ.*, **115**, 2547–2563, https://doi.org/10.1016/j.rse.2011.05.012.

Beguería, S., S. M. Vicente-Serrano, F. Reig, and B. Latorre, 2014: Standardized precipitation evapotranspiration index (SPEI) revisited: Parameter fitting, evapotranspiration models, tools, datasets and drought monitoring. *Int. J. Climatol.*, **34**, 3001–3023, https://doi.org/10.1002/joc.3887.

Bouchet, R. J., 1963: Evapotranspiration réelle evapotranspiration potentielle, signification climatique. *IAHS Publ.*, **62**, 134–142.

Breshears, D. D., H. D. Adams, D. Eamus, M. G. McDowell, D. J. Law, R. E. Will, A. P. Williams, and C. B. Zou, 2013: The critical amplifying role of increasing atmospheric moisture demand on tree mortality and associated regional die-off. *Front. Plant Sci.*, **4**, 266, https://doi.org/10.3389/fpls.2013.00266.

Brümmer, C., and Coauthors, 2012: How climate and vegetation type influence evapotranspiration and water use efficiency in Canadian forest, peatland and grassland ecosystems. *Agric. For. Meteor.*, **153**, 14–30, https://doi.org/10.1016/j.agrformet.2011.04.008.

Budyko, M. I., 1948: *Evaporation under Natural Conditions*. Gidrometeoizdat, 136 pp.

Chaves, M. M., J. P. Maroco, and J. S. Pereira, 2003: Understanding plant responses to drought—From genes to the whole plant. *Funct. Plant Biol.*, **30**, 239–264, https://doi.org/10.1071/FP02076.

Chen, T., G. Xia, T. Liu, W. Chen, and D. Chi, 2016: Assessment of drought impact on main cereal crops using a standardized precipitation evapotranspiration index in Liaoning Province, China. *Sustainability*, **8**, 1069, https://doi.org/10.3390/su8101069.

Choat, B., and Coauthors, 2012: Global convergence in the vulnerability of forests to drought. *Nature*, **491**, 752–755, https://doi.org/10.1038/nature11688.

Ciais, P., and Coauthors, 2005: Europe-wide reduction in primary productivity caused by the heat and drought in 2003. *Nature*, **437**, 529–533, https://doi.org/10.1038/nature03972.

Donohue, R. J., T. R. McVicar, and M. L. Roderick, 2010: Assessing the ability of potential evaporation formulations to capture the dynamics in evaporative demand within a changing climate. *J. Hydrol.*, **386**, 186–197, https://doi.org/10.1016/j.jhydrol.2010.03.020.

——, and Coauthors, 2014: Evaluation of the remote-sensing-based DIFFUSE model for estimating photosynthesis of vegetation. *Remote Sens. Environ.*, **155**, 349–365, https://doi.org/10.1016/j.rse.2014.09.007.

Duncan, J., D. Stow, J. Franklin, and A. Hope, 1993: Assessing the relationship between spectral vegetation indices and shrub cover in the Jordana Basin, New Mexico. *Int. J. Remote Sens.*, **14**, 3395–3416, https://doi.org/10.1080/01431169308904454.

Espadafor, M., I. J. Lorite, P. Gavilán, and J. Berengena, 2011: An analysis of the tendency of reference evapotranspiration estimates and other climate variables during the last 45 years in southern Spain. *Agric. Water Manage.*, **98**, 1045–1061, https://doi.org/10.1016/j.agwat.2011.01.015.

Fisher, J. B., K. P. Tu, and D. D. Baldocchi, 2008: Global estimates of the land–atmosphere water flux based on monthly AVHRR and ISLSCP-II data, validated at 16 FLUXNET sites. *Remote Sens. Environ.*, **112**, 901–919, https://doi.org/10.1016/j.rse.2007.06.025.

——, R. J. Whittaker, and Y. Malhi, 2011: ET come home: Potential evapotranspiration in geographical ecology. *Global Ecol. Biogeogr.*, **20**, 1–18, https://doi.org/10.1111/j.1466-8238.2010.00578.x.

——, and Coauthors, 2017: The future of evapotranspiration: Global requirements for ecosystem functioning, carbon and climate feedbacks, agricultural management, and water resources. *Water Resour. Res.*, **53**, 2618–2626, https://doi.org/10.1002/2016WR020175.

Gash, J. H. C., 1979: An analytical model of rainfall interception by forests. *Quart. J. Roy. Meteor. Soc.*, **105**, 43–55, https://doi.org/10.1002/qj.49710544304.

Gillies, R. R., W. P. Kustas, and K. S. Humes, 1997: A verification of the 'triangle' method for obtaining surface soil water content and energy fluxes from remote measurements of the normalized difference vegetation index (NDVI) and surface radiant temperature. *Int. J. Remote Sens.*, **18**, 3145–3166, https://doi.org/10.1080/014311697217026.

Greenwood, S., and Coauthors, 2017: Tree mortality across biomes is promoted by drought intensity, lower wood density and higher specific leaf area. *Ecol. Lett.*, **20**, 539–553, https://doi.org/10.1111/ele.12748.

Gutman, G. G., 1991: Vegetation indices from AVHRR: An update and future prospects. *Remote Sens. Environ.*, **35**, 121–136, https://doi.org/10.1016/0034-4257(91)90005-Q.

Guttman, N. B., 1999: Accepting the standardized precipitation index: A calculation algorithm. *J. Amer. Water Resour. Assoc.*, **35**, 311–322, https://doi.org/10.1111/j.1752-1688.1999.tb03592.x.

Harris, I., P. D. Jones, T. J. Osborn, and D. H. Lister, 2014: Updated high-resolution grids of monthly climatic observations—The CRU TS3.10 dataset. *Int. J. Climatol.*, **34**, 623–642, https://doi.org/10.1002/joc.3711.

Heim, R. R., Jr., 2002: A review of twentieth-century drought indices used in the United States. *Bull. Amer. Meteor. Soc.*, **83**, 1149–1166, https://doi.org/10.1175/1520-0477-83.8.1149.

Hobbins, M. T., A. Wood, D. J. McEvoy, J. L. Huntington, C. Morton, M. Anderson, and C. Hain, 2016: The evaporative demand drought index. Part I: Linking drought evolution to variations in evaporative demand. *J. Hydrometeor.*, **17**, 1745–1761, https://doi.org/10.1175/JHM-D-15-0121.1.

Hosking, J. R. M., 1990: L-moments: Analysis and estimation of distributions using linear combinations of order statistics. *J. Roy. Stat. Soc.* **52B**, 105–124.

Ji, L., and A. J. Peters, 2003: Assessing vegetation response to drought in the northern Great Plains using vegetation and drought indices. *Remote Sens. Environ.*, **87**, 85–98, https://doi.org/10.1016/S0034-4257(03)00174-3.

Katerji, N., and G. Rana, 2011: Crop reference evapotranspiration: A discussion of the concept, analysis of the process and validation. *Water Resour. Manage.*, **25**, 1581–1600, https://doi.org/10.1007/s11269-010-9762-1.

Keyantash, J., and J. A. Dracup, 2002: The quantification of drought: An evaluation of drought indices. *Bull. Amer. Meteor. Soc.*, **83**, 1167–1180, https://doi.org/10.1175/1520-0477-83.8.1167.

Kim, D., and J. Rhee, 2016: A drought index based on actual evapotranspiration from the Bouchet hypothesis. *Geophys. Res. Lett.*, **43**, 10 277–10 285, https://doi.org/10.1002/2016GL070302.

Kogan, F. N., 1997: Global drought watch from space. *Bull. Amer. Meteor. Soc.*, **78**, 621–636, https://doi.org/10.1175/1520-0477(1997)078<0621:GDWFS>2.0.CO;2.

Labudová, L., M. Labuda, and A. Takáč , 2017: Comparison of SPI and SPEI applicability for drought impact assessment on crop production in the Danubian lowland and the east Slovakian lowland. *Theor. Appl. Climatol.*, **128**, 491–506, https://doi.org/10.1007/s00704-016-1870-2.

Leuning, R., 1995: A critical appraisal of a combined stomatal-photosynthesis model for C_3 plants. *Plant Cell Environ.*, **18**, 339–335, https://doi.org/10.1111/j.1365-3040.1995.tb00370.x.

Liu, W. T., and F. N. Kogan, 1996: Monitoring regional drought using the vegetation condition index. *Int. J. Remote Sens.*, **17**, 2761–2782, https://doi.org/10.1080/01431169608949106.

Lloyd-Hughes, B., 2014: The impracticality of a universal drought definition. *Theor. Appl. Climatol.*, **117**, 607–611, https://doi.org/10.1007/s00704-013-1025-7.

Lobell, D. B., M. Bänziger, C. Magorokosho, and B. Vivek, 2011: Nonlinear heat effects on African maize as evidenced by historical yield trials. *Nat. Climate Change*, **1**, 42–45, https://doi.org/10.1038/nclimate1043.

López-Moreno, J. I., S. M. Vicente-Serrano, J. Zabalza, S. Beguería, J. Lorenzo-Lacruz, C. Azorin-Molina, and E. Morán-Tejeda, 2013: Hydrological response to climate variability at different time scales: A study in the Ebro basin. *J. Hydrol.*, **477**, 175–188, https://doi.org/10.1016/j.jhydrol.2012.11.028.

Lorenzo-Lacruz, J., S. M. Vicente-Serrano, J. C. González-Hidalgo, J. I. López-Moreno, and N. Cortesi, 2013: Hydrological drought response to meteorological drought at various time scales in the Iberian Peninsula. *Climate Res.*, **58**, 117–131, https://doi.org/10.3354/cr01177.

Ma, M., L. Ren, F. Yuan, S. Jiang, Y. Liu, H. Kong, and L. Gong, 2014: A new standardized Palmer drought index for hydro-meteorological use. *Hydrol. Processes*, **28**, 5645–5661, https://doi.org/10.1002/hyp.10063.

Martens, B., and Coauthors, 2017: GLEAM v3: Satellite-based land evaporation and root-zone soil moisture. *Geosci. Model Dev.*, **10**, 1903–1925, https://doi.org/10.5194/gmd-10-1903-2017.

McCabe, M. F., A. Ershadi, C. Jimenez, D. G. Miralles, D. Michel, and E. F. Wood, 2016: The GEWEX LandFlux project: Evaluation of model evaporation using tower-based and globally gridded forcing data. *Geosci. Model Dev.*, **9**, 283–305, https://doi.org/10.5194/gmd-9-283-2016.

——, and Coauthors, 2017: The future of Earth observation in hydrology. *Hydrol. Earth Syst. Sci.*, **21**, 3879–3914, https://doi.org/10.5194/hess-21-3879-2017.

McDowell, N., and Coauthors, 2008: Mechanisms of plant survival and mortality during drought: Why do some plants survive while others succumb to drought? *New Phytol.*, **178**, 719–739, https://doi.org/10.1111/j.1469-8137.2008.02436.x.

McEvoy, D. J., J. L. Huntington, J. T. Abatzoglou, and L. M. Edwards, 2012: An evaluation of multiscalar drought indices in Nevada and eastern California. *Earth Interact.*, **16**, https://doi.org/10.1175/2012EI000447.1.

——, ——, M. T. Hobbins, A. Wood, C. Morton, M. Anderson, and C. Hain, 2016a: The evaporative demand drought index. Part II: CONUS-wide assessment against common drought indicators. *J. Hydrometeor.*, **17**, 1763–1779, https://doi.org/10.1175/JHM-D-15-0122.1.

——, ——, J. F. Mejia, and M. T. Hobbins, 2016b: Improved seasonal drought forecasts using reference evapotranspiration anomalies. *Geophys. Res. Lett.*, **43**, 377–385, https://doi.org/10.1002/2015GL067009.

McKee, T. B., N. J. Doesken, and J. Kleist, 1993: The relationship of drought frequency and duration to time scales. *Proc. Eighth Conf. on Applied Climatology*, Anaheim, CA, Amer. Meteor. Soc, 179–184.

McVicar, T. R., and D. L. B. Jupp, 1998: The current and potential operational uses of remote sensing to aid decisions on drought exceptional circumstances in Australia: A review. *Agric. Syst.*, **57**, 399–468, https://doi.org/10.1016/S0308-521X(98)00026-2.

——, T. G. Van Niel, L. T. Li, M. L. Roderick, D. P. Rayner, L. Ricciardulli, and R. J. Donohue, 2008: Wind speed climatology and trends for Australia, 1975–2006: Capturing the stilling phenomenon and comparison with near-surface reanalysis output. *Geophys. Res. Lett.*, **35**, L20403, https://doi.org/10.1029/2008GL035627.

——, M. L. Roderick, R. J. Donohue, and T. G. Van Niel, 2012a: Less bluster ahead? Ecohydrological implications of global trends of terrestrial near-surface wind speeds. *Ecohydrology*, **5**, 381–388, https://doi.org/10.1002/eco.1298.

——, and Coauthors, 2012b: Global review and synthesis of trends in observed terrestrial near-surface wind speeds: Implications for evaporation. *J. Hydrol.*, **416–417**, 182–205, https://doi.org/10.1016/j.jhydrol.2011.10.024.

Michel, D., and Coauthors, 2016: The WACMOS-ET project—Part 1: Tower-scale evaluation of four remote-sensing-based evapotranspiration algorithms. *Hydrol. Earth Syst. Sci.*, **20**, 803–822, https://doi.org/10.5194/hess-20-803-2016.

Miralles, D. G., T. R. H. Holmes, R. A. M. De Jeu, J. H. Gash, A. G. C. A. Meesters, and A. J. Dolman, 2011: Global land-surface evaporation estimated from satellite-based observations. *Hydrol. Earth Syst. Sci.*, **15**, 453–469, https://doi.org/10.5194/hess-15-453-2011.

——, and Coauthors, 2016: The WACMOS-ET project—Part 2: Evaluation of global terrestrial evaporation data sets. *Hydrol. Earth Syst. Sci.*, **20**, 823–842, https://doi.org/10.5194/hess-20-823-2016.

Mishra, A.K., and V. P Singh, 2010: A review of drought concepts. *J. Hydrol.*, **391**, 202–216, https://doi.org/10.1016/j.jhydrol.2010.07.012.

Morton, F. I., 1983: Operational estimates of areal evapotranspiration and their significance to the science and practice of hydrology. *J. Hydrol.*, **66**, 1–76, https://doi.org/10.1016/0022-1694(83)90177-4.

Mu, Q., M. Zhao, and S. W. Running, 2011: Improvements to a MODIS global terrestrial evapotranspiration algorithm. *Remote Sens. Environ.*, **115**, 1781–1800, https://doi.org/10.1016/j.rse.2011.02.019.

Narasimhan, B., and R. Srinivasan, 2005: Development and evaluation of soil moisture deficit index (SMDI) and

evapotranspiration deficit index (ETDI) for agricultural drought monitoring. *Agric. For. Meteor.*, **133**, 69–88, https://doi.org/10.1016/j.agrformet.2005.07.012.

Otkin, J. A., and Coauthors, 2016: Assessing the evolution of soil moisture and vegetation conditions during the 2012 United States flash drought. *Agric. For. Meteor.*, **218–219**, 230–242, https://doi.org/10.1016/j.agrformet.2015.12.065.

Palmer, W. C., 1965: Meteorological droughts. U.S. Department of Commerce Weather Bureau Research Paper 45, 58 pp.

Papagiannopoulou, C., D. G. Miralles, W. A. Dorigo, N. E. C. Verhoest, M. Depoorter, and W. Waegeman, 2017: Vegetation anomalies caused by antecedent precipitation in most of the world. *Environ. Res. Lett.*, **12**, 074016, https://doi.org/10.1088/1748-9326/aa7145.

Páscoa, P., C. M. Gouveia, A. Russo, and R. M. Trigo, 2017: The role of drought on wheat yield interannual variability in the Iberian Peninsula from 1929 to 2012. *Int. J. Biometeorol.*, **61**, 439–451, https://doi.org/10.1007/s00484-016-1224-x.

Pasho, E., J. J. Camarero, M. de Luis, and S. M. Vicente-Serrano, 2011: Impacts of drought at different time scales on forest growth across a wide climatic gradient in north-eastern Spain. *Agric. For. Meteor.*, **151**, 1800–1811, https://doi.org/10.1016/j.agrformet.2011.07.018.

Penman, H. L., 1948: Natural evaporation from open water, bare soil and grass. *Proc. Roy. Soc. London*, **193A**, 120–146, https://doi.org/10.1098/rspa.1948.0037.

Perdigão, J. C., R. Salgado, M. J. Costa, H. P. Dasari, and A. Sanchez-Lorenzo, 2016: Variability and trends of downward surface global solar radiation over the Iberian Peninsula based on ERA-40 reanalysis. *Int. J. Climatol.*, **36**, 3917–3933, https://doi.org/10.1002/joc.4603.

Pinzon, J. E., and C. J. Tucker, 2014: A non-stationary 1981–2012 AVHRR $NDVI_{3g}$ time series. *Remote Sens.*, **6**, 6929–6960, https://doi.org/10.3390/rs6086929.

Priestley, C. H. B., and R. J. Taylor, 1972: On the assessment of surface heat flux and evaporation using large-scale parameters. *Mon. Wea. Rev.*, **100**, 81–92, https://doi.org/10.1175/1520-0493(1972)100<0081:OTAOSH>2.3.CO;2.

Quiring, S. M., and T. N. Papakryiakou, 2003: An evaluation of agricultural drought indices for the Canadian prairies. *Agric. For. Meteor.*, **118**, 49–62, https://doi.org/10.1016/S0168-1923(03)00072-8.

Rosas, T., L. Galiano, R. Ogaya, J. Peñuelas, and J. Martínez-Vilalta, 2013: Dynamics of non-structural carbohydrates in three Mediterranean woody species following long-term experimental drought. *Front. Plant Sci.*, **4**, 400, https://doi.org/10.3389/fpls.2013.00400.

Rotstayn, L. D., M. L. Roderick, and G. D. Farquhar, 2006: A simple pan-evaporation model for analysis of climate simulations: Evaluation over Australia. *Geophys. Res. Lett.*, **33**, L17715, https://doi.org/10.1029/2006GL027114.

Simelton, E., E. D. G. Fraser, M. Termansen, P. M. Forster, and A. J. Dougill, 2009: Typologies of crop-drought vulnerability: An empirical analysis of the socio-economic factors that influence the sensitivity and resilience to drought of three major food crops in China (1961–2001). *Environ. Sci. Policy*, **12**, 438–452, https://doi.org/10.1016/j.envsci.2008.11.005.

Stagge, J. H., L. M. Tallaksen, L. Gudmundsson, A. F. Van Loon, and K. Stahle, 2015: Candidate distributions for climatological drought indices (SPI and SPEI). *Int. J. Climatol.*, **35**, 4027–4040, https://doi.org/10.1002/joc.4267.

Stahl, K., I. Kohn, L. De Stefano, L. M. Tallaksen, F. C. Rego, S. I. Seneviratne, J. Andreu, and H. A. J. van Lanen, 2015: An impact perspective on pan-European drought sensitivity. *Drought: Research and Science-Policy Interfacing*, J. Andreu et al., Eds., CRC Press, 329–334.

——, and Coauthors, 2016: Impacts of European drought events: Insights from an international database of text-based reports. *Nat. Hazards Earth Syst. Sci.*, **16**, 801–819, https://doi.org/10.5194/nhess-16-801-2016.

Stephenson, N. L., 1990: Climatic control of vegetation distribution: The role of the water balance. *Amer. Nat.*, **135**, 649–670, https://doi.org/10.1086/285067.

——, 1998: Actual evapotranspiration and deficit: Biologically meaningful correlates of vegetation distribution across spatial scales. *J. Biogeogr.*, **25**, 855–870, https://doi.org/10.1046/j.1365-2699.1998.00233.x.

Tucker, C. J., C. Vanpraet, E. Boerwinkel, and A. Gaston, 1983: Satellite remote sensing of total dry matter production in the Senegalese Sahel. *Remote Sens. Environ.*, **13**, 461–474, https://doi.org/10.1016/0034-4257(83)90053-6.

Van Loon, A. F., 2015: Hydrological drought explained. *Wiley Interdiscip. Rev.: Water*, **2**, 359–392, https://doi.org/10.1002/wat2.1085.

——, and Coauthors, 2016: Drought in a human-modified world: Reframing drought definitions, understanding, and analysis approaches. *Hydrol. Earth Syst. Sci.*, **20**, 3631–3650, https://doi.org/10.5194/hess-20-3631-2016.

Vicente-Serrano, S. M., 2006: Differences in spatial patterns of drought on different time scales: An analysis of the Iberian Peninsula. *Water Resour. Manage.*, **20**, 37–60, https://doi.org/10.1007/s11269-006-2974-8.

——, 2016: Foreword: Drought complexity and assessment under climate change conditions. *Cuad. Invest. Geogr.*, **42**, 7–11, https://doi.org/10.18172/cig.2961.

——, 2018: A global dataset of the standardized evapotranspiration deficit index (SEDI) (1964–2014). DIGITAL.CSIC, accessed 4 May 2018, https://doi.org/10.20350/digitalCSIC/8529.

——, and S. Beguería, 2016: Comment on 'Candidate distributions for climatological drought indices (SPI and SPEI)' by James H. Stagge et al. *Int. J. Climatol.*, **36**, 2120–2131, https://doi.org/10.1002/joc.4474.

——, ——, and J. I. López-Moreno, 2010a: A multiscalar drought index sensitive to global warming: The standardized precipitation evapotranspiration index. *J. Climate*, **23**, 1696–1718, https://doi.org/10.1175/2009JCLI2909.1.

——, ——, ——, M. Angulo, and A. El Kenawy, 2010b: A new global 0.5° gridded dataset (1901–2006) of a multiscalar drought index: Comparison with current drought index datasets based on the Palmer drought severity index. *J. Hydrometeor.*, **11**, 1033–1043, https://doi.org/10.1175/2010JHM1224.1.

——, ——, and ——, 2011: Comment on "Characteristics and trends in various forms of the Palmer drought severity index (PDSI) during 1900–2008" by Aiguo Dai. *J. Geophys. Res.*, **116**, D19112, https://doi.org/10.1029/2011JD016410.

——, and Coauthors, 2012a: Performance of drought indices for ecological, agricultural, and hydrological applications. *Earth Interact.*, **16**, https://doi.org/10.1175/2012EI000434.1.

——, J. I. López-Moreno, S. Beguería, J. Lorenzo-Lacruz, C. Azorin-Molina, and E. Morán-Tejeda, 2012b: Accurate computation of a streamflow drought index. *J. Hydrol. Eng.*, **17**, 318–332, https://doi.org/10.1061/(ASCE)HE.1943-5584.0000433.

——, and Coauthors, 2013: The response of vegetation to drought time-scales across global land biomes. *Proc. Natl. Acad. Sci. USA*, **110**, 52–57, https://doi.org/10.1073/pnas.1207068110.

——, C. Azorin-Molina, A. Sanchez-Lorenzo, J. Revuelto, J. I. López-Moreno, J. C. González-Hidalgo, E. Moran-Tejeda,

and F. Espejo, 2014: Reference evapotranspiration variability and trends in Spain, 1961–2011. *Global Planet. Change*, **121**, 26–40, https://doi.org/10.1016/j.gloplacha.2014.06.005.

——, J. J. Camarero, J. Zabalza, G. Sangüesa-Barreda, J. I. López-Moreno, and C. L. Tague, 2015: The evapotranspiration deficit controls growth and net primary production: Implications for Circum-Mediterranean forests under forecasted warmer and drier conditions. *Agric. For. Meteor.*, **206**, 45–54, https://doi.org/10.1016/j.agrformet.2015.02.017.

——, and Coauthors, 2017: Recent changes of relative humidity: Regional connection with land and ocean processes. *Earth Syst. Dyn. Discuss.*, https://doi.org/10.5194/esd-2017-43.

Wang, K., Z. Li, and M. Cribb, 2006: Estimation of evaporative fraction from a combination of day and night land surface temperatures and NDVI: A new method to determine the Priestley–Taylor parameter. *Remote Sens. Environ.*, **102**, 293–305, https://doi.org/10.1016/j.rse.2006.02.007.

Wang, W., W. Xing, and Q. Shao, 2015: How large are uncertainties in future projection of reference evapotranspiration through different approaches? *J. Hydrol.*, **524**, 696–700, https://doi.org/10.1016/j.jhydrol.2015.03.033.

Wilhite, D. A., Ed., 1993: *Drought Assessment, Management, and Planning: Theory and Case Studies*. Springer, 293 pp.

——, 2000: Drought as a natural hazard: Concepts and definitions. *Drought: A Global Assessment*, D. A. Wilhite, Ed., Vol. 1, Routledge, 3–18.

Will, R. E., S. M. Wilson, C. B. Zou, and T. C. Hennessey, 2013: Increased vapor pressure deficit due to higher temperature leads to greater transpiration and faster mortality during drought for tree seedlings common to the forest-grassland ecotone. *New Phytol.*, **200**, 366–374, https://doi.org/10.1111/nph.12321.

Willett, K. M., R. J. H. Dunn, P. W. Thorne, S. Bell, M. de Podesta, D. E. Parker, P. D. Jones, and C. N. Williams Jr., 2014: HadISDH land surface multi-variable humidity and temperature record for climate monitoring. *Climate Past*, **10**, 1983–2006, https://doi.org/10.5194/cp-10-1983-2014.

Yang, Y. T., R. J. Donohue, T. R. McVicar, and M. L. Roderick, 2015: An analytical model for relating global terrestrial carbon assimilation with climate and surface conditions using a rate limitation framework. *Geophys. Res. Lett.*, **42**, 9825–9835, https://doi.org/10.1002/2015GL066835.

——, T. R. McVicar, R. J. Donohue, Y. Zhang, M. L. Roderick, F. H. S. Chiew, L. Zhang, and J. Zhang, 2017: Lags in hydrologic recovery following an extreme drought: Assessing the roles of climate and catchment characteristics. *Water Resour. Res.*, **53**, 4821–4837, https://doi.org/10.1002/2017WR020683.

Yao, Y., S. Liang, Q. Qin, and K. Wang, 2010: Monitoring drought over the conterminous United States using MODIS and NCEP Reanalysis-2 data. *J. Appl. Meteor. Climatol.*, **49**, 1665–1680, https://doi.org/10.1175/2010JAMC2328.1.

Zampieri, M., F. D'Andrea, R. Vautard, P. Ciais, N. de Noblet-Ducoudré, and P. Yiou, 2009: Hot European summers and the role of soil moisture in the propagation of Mediterranean drought. *J. Climate*, **22**, 4747–4758, https://doi.org/10.1175/2009JCLI2568.1.

Zhang, Q., D. Kong, V. P. Singh, and P. Shi, 2017: Response of vegetation to different time-scales drought across China: Spatiotemporal patterns, causes and implications. *Global Planet. Change*, **152**, 1–11, https://doi.org/10.1016/j.gloplacha.2017.02.008.

Zhang, Y., and Coauthors, 2016: Multi-decadal trends in global terrestrial evapotranspiration and its components. *Sci. Rep.*, **6**, 19124, https://doi.org/10.1038/srep19124.

Zipper, S. C., J. Qiu, and C. J. Kucharik, 2016: Drought effects on US maize and soybean production: Spatiotemporal patterns and historical changes. *Environ. Res. Lett.*, **11**, 094021, https://doi.org/10.1088/1748-9326/11/9/094021.